 doi:10.1111/j.1525-1314.2011.00950.x

Petrological consequences of variations in metamorphic reaction affinity

D. R. M. PATTISON,[1] C. DE CAPITANI[2] AND F. GAIDIES[1,3]
[1]Department of Geoscience, University of Calgary, Calgary, AB T2N 1N4, Canada (pattison@ucalgary.ca)
[2]Mineralogisch-Petrographisches Institut, Universität Basel, Bernoullistrasse 30, 4056 Basel, Switzerland
[3]Department of Earth Sciences, Carleton University, 1125 Colonel By Drive, Ottawa, ON K1S 5B6, Canada

ABSTRACT The extent to which kinetic barriers to nucleation and growth delay the onset of prograde metamorphic reaction, commonly known as overstepping, is related to the macroscopic driving force for reaction, termed reaction affinity. Reaction affinity is defined in the context of overstepping as the Gibbs free-energy difference between the thermodynamically stable, but not-yet-crystallized, products and the metastable reactants. Mineral reactions which release large quantities of H_2O, such as chlorite-consuming reactions, have a higher entropy/volume change, and therefore a higher reaction affinity per unit of temperature/pressure overstep, than those which release little or no H_2O. The former are expected to be overstepped in temperature or pressure less than the latter. Different methods of calculating reaction affinity are discussed. Reaction affinity 'maps' are calculated that graphically portray variations in reaction affinity on equilibrium phase diagrams, allowing predictions to be made about expected degrees of overstepping. Petrological consequences of variations in reaction affinity include: (i) metamorphic reaction intervals may be discrete rather than continuous, especially in broad multivariant domains across which reaction affinity builds slowly; (ii) reaction intervals may not correspond in a simple way to reaction boundaries and domains in an equilibrium phase diagram, and may involve metastable reactions; (iii) overstepping can lead to a 'cascade effect', in which several stable and metastable reactions involving the same reactant phases proceed simultaneously; (iv) fluid generation, and possibly fluid presence in general, may be episodic rather than continuous, corresponding to discrete intervals of reaction; (v) overstepping related to slowly building reaction affinity in multivariant reaction intervals may account for the commonly abrupt development in the field of certain index mineral isograds; and (vi) *P–T* estimation based on combined use of phase diagram sections and mineral modes/compositions on the one hand, and classical thermobarometry methods on the other, may not agree even if the same thermodynamic data are used. Natural examples of the above, both contact and regional, are provided. The success of the metamorphic facies principle suggests that these kinetic effects are second-order features that operate within a broadly equilibrium approach to metamorphism. However, it may be that the close approach to equilibrium occurs primarily at the boundaries between the metamorphic facies, corresponding to discrete intervals of high entropy, dehydration reaction involving consumption of hydrous phases like chlorite (greenschist–amphibolite facies boundary) and mica (amphibolite–granulite facies boundary), and less so within the facies themselves. The results of this study suggest that it is important to consider the possibility of reactions removed from equilibrium when inferring the *P–T–t* evolution of metamorphic rocks.

Key words: kinetics; metamorphic facies; metamorphic reactions; reaction affinity; reaction overstepping.

INTRODUCTION

Understanding the interplay between the approach to equilibrium and reaction kinetics is one of the central challenges of metamorphic petrology. The equilibrium model for prograde metamorphism is founded on the metamorphic facies principle (Eskola, 1915), which has as its elements the predictable relationship between mineral assemblage and bulk composition, repeated occurrences of the same suite of minerals in rocks of different bulk composition that experienced the same *P–T* conditions, and the repeatability of metamorphic mineral assemblage zones in similar settings the world over (e.g. the common prograde sequence of garnet, staurolite, kyanite & sillimanite zones in Barrovian metamorphic settings). Such regularity would not be expected if disequilibrium processes were the primary determinant of metamorphic mineral assemblage development.

Set against the equilibrium view of prograde metamorphism is the recognition that, for any metamorphic process to occur, at least some departure from equilibrium (overstepping) is required to exceed the activation energy barriers to nucleation, dissolution

and growth. The two views may be reconciled if the departure from equilibrium is sufficiently small, or rare, that it does not compromise the regularity noted above. Published estimates of the degree of overstepping of metamorphic reactions vary according to assumptions about which of the three main kinetic components of a metamorphic reaction – nucleation, interface reaction (dissolution and growth) and intergranular transport – are rate limiting. Even though this distinction is a simplification (for example, nucleation and growth cannot occur without transport), one process usually dominates the overall reaction kinetics. Of the three, only nucleation has the capability of imposing a finite requirement for overstepping (a critical overstepping), as there may be a significant interval beyond the equilibrium condition where the probability of a nucleation event is effectively zero (Ridley & Thompson, 1986). Once nucleation has initiated, however, it is unlikely to continue to be rate limiting, owing to the exponential increase in nucleation rate with temperature overstep (Ridley & Thompson, 1986; Rubie, 1998; Waters & Lovegrove, 2002). Interface reaction and transport have a real rate of progress at any degree of overstepping, so the question becomes at what level of overstepping the progress becomes macroscopically observable.

Based on experimental rates of interface reaction, without consideration of the nucleation and transport steps, Walther & Wood (1984) argued that overstepping during prograde metamorphism would amount to only a few (<10) degree Celsius for normal devolatilization reactions in contact and regional settings, ranging up to ~40 °C for certain solid–solid reactions in contact aureoles. Lasaga (1986) and Lasaga & Rye (1993), based on similar assumptions, argued for somewhat greater degrees of overstepping, introducing the idea of kinetically controlled isograds that preserve the sequence of equilibrium isograds but are overstepped to varying degrees.

Ridley & Thompson (1986), Waters (1990) and Rubie (1998) argued that nucleation difficulty might be the primary determinant of degree of overstepping in prograde metamorphism, based on the marked difference in reaction progress between seeded and unseeded phase equilibrium experiments, and on a number of natural examples. Subsequent studies of natural settings came to a similar conclusion (Manning *et al.*, 1993; Waters & Lovegrove, 2002; Zeh & Holness, 2003; Wilbur & Ague, 2006; Pattison & Tinkham, 2009). In these studies, the range of suggested nucleation-related overstepping varied from 30 to 80 °C, with the high end of the range either for rocks in the inner contact zones of hot intrusions (Manning *et al.*, 1993) or in atypical bulk compositions (Zeh & Holness, 2003).

Rubie (1986) and Ridley & Thompson (1986) emphasized the additional importance of fluid presence or absence to reaction kinetics. The kinetic role of fluid is different from the thermodynamic role of fluid, whether as a phase whose presence or absence may determine if certain reactions can proceed (e.g. hydration reactions – see extensive discussion in Guiraud *et al.*, 2001), or as a chemically reactive agent that, if out of equilibrium with the rock it encounters, can drive metamorphic reaction (e.g. Ferry, 1988, 1991, 1994; Ferry & Gerdes, 1998). Fluids (especially aqueous) provide a medium for enhanced mass transfer by diffusion or advection in solution, and may assist interface processes by providing other mechanisms for attachment and detachment. The effects of fluids on nucleation are less well understood, but could include helping embryo development through easier nano-scale mass transfer, and perhaps modifying substrates to make cluster assembly more likely (D. J. Waters, written comm., 2011). Fluid presence has been shown to significantly lower degrees of overstepping, as revealed spectacularly in interlayered eclogites and granulites in Holsnoy, Norway (Austrheim, 1987), and more subtly in interlayered andalusite-bearing and andalusite-free metapelites in the Nelson aureole, British Columbia (Pattison & Tinkham, 2009). In summary, despite the overall success of the metamorphic facies principle, there is evidence that kinetics play a non-negligible role in controlling reaction onset and progress within the relatively broad P–T domains represented by the metamorphic facies, and in some circumstances may cause sufficiently severe departures from equilibrium that the metamorphic facies concept is violated.

The extent to which kinetic barriers to nucleation and growth delay the onset of reaction is related to the macroscopic energetic driving force for reaction, termed reaction affinity, A (de Donder, 1922, 1936; Prigogine & Defay, 1954; International Union of Pure and Applied Chemistry (IUPAC), 2011) (http://en.wikipedia.org/wiki/Chemical_affinity, http://en.wikipedia.org/wiki/IUPAC). These workers considered reaction affinity in the context of a mixture of reactive chemical species at constant pressure and temperature. de Donder (1922, 1936) defined reaction affinity as the negative of the Gibbs free energy of reaction, i.e. $A = -\Delta_r G_{P,T}$, whereas the 2011 IUPAC definition of reaction affinity, closely modelled on the work of Prigogine & Defay (1954), is the negative partial derivative of Gibbs free energy with respect to extent of reaction, ξ, i.e:

$$A = -\left|\frac{\partial G}{\partial \xi}\right|_{P,T}.$$

In this article, we are concerned with reaction overstepping during prograde metamorphism caused by changes in temperature and, to a lesser degree, pressure and fluid composition. In this context, we define reaction affinity as the negative of the Gibbs free-energy difference between the thermodynamically stable, but not-yet-crystallized, products and the metastable reactants (see Figs 1 & 2). Although this definition is most relevant to the critical overstep

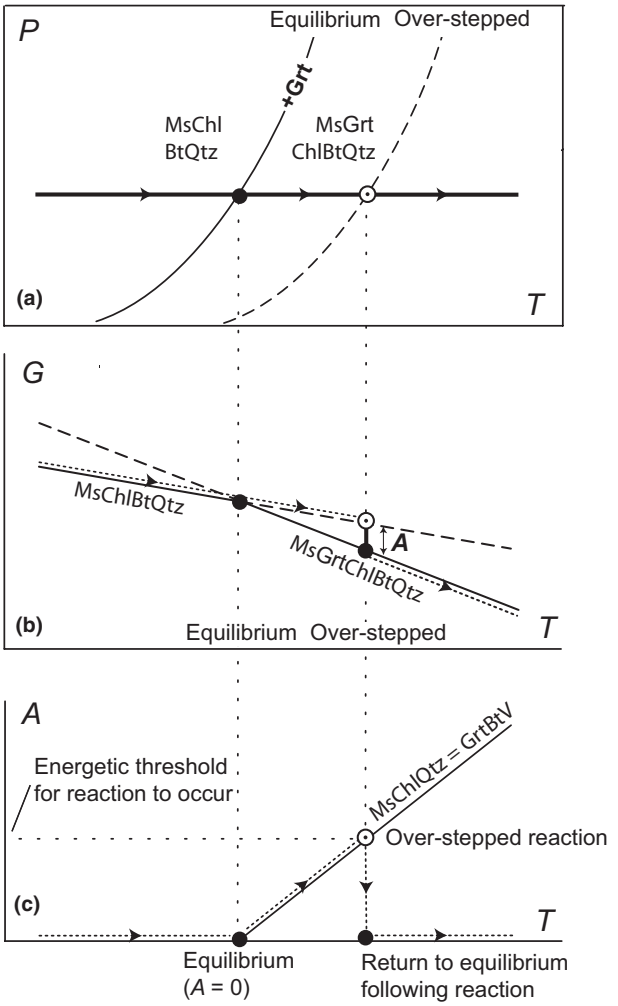

Fig. 1. Reaction overstepping illustrated on: (a) schematic pressure–temperature phase equilibrium (*P–T*) diagram; (b) free energy–temperature (*G–T*) diagram; and (c) reaction affinity–temperature (*A–T*) diagram. Mineral abbreviations from Kretz (1983). V = H_2O fluid.

associated with nucleation, once the new phase has nucleated, the affinity that accumulated to achieve nucleation drives the total reaction (interface processes and local mass transfer). The above definition may therefore provide a limiting (maximum) condition for reaction affinity associated with overstepping in situations where nucleation is not rate limiting (more discussion below).

Reaction affinity is explicitly incorporated in the general kinetic rate equation:

$$\text{Rate} = F^*(1 - \exp(A/RT))^*\exp(-G_{\text{act}}/RT), \quad (1)$$

in which Rate is the amount of material produced in unit time, F is a pre-exponential factor, A is the reaction affinity, R is the universal gas constant, T is temperature in Kelvin and G_{act} is the activation energy barrier to an unspecified rate-limiting kinetic process (e.g. nucleation, transport, interface reaction). Whereas the rates

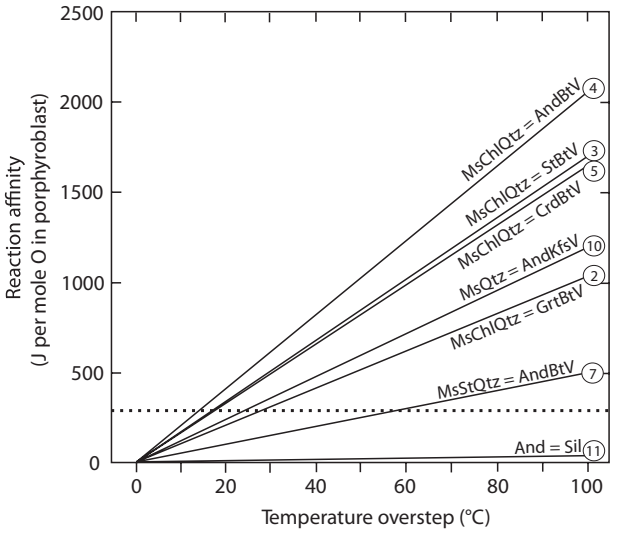

Fig. 2. Quantitative reaction affinity–temperature (*A–T*) trends for different reactions, calculated per mole of oxygen in the product porphyroblast. The temperature axis is temperature overstep. The slopes of the reactions are the reaction entropies, and are listed in Table 1. See text for method of calculation. Mineral abbreviations from Kretz (1983). V = H_2O fluid.

of transport and interface reaction increase steadily with temperature, the same cannot be said for reaction affinity because every reaction interval that a rock traverses along its *P–T* path involves a different free-energy change. If the reaction affinity builds up markedly with overstep, overstepping is expected to be small, whereas if it builds up modestly, reaction may be delayed or not occur at all.

The purpose of this article is to explore the petrological consequences of variations of reaction affinity, in particular it's bearing on the extent to which metamorphism can be viewed as following a continuous path through successive equilibrium states (the equilibrium model). The first part of the article is concerned with general strategies for calculating reaction affinity. *P–T* 'maps' of reaction affinity are then presented that can be used in concert with equilibrium phase diagrams to predict where reaction is expected to be overstepped or not. The second part of the article explores some of the petrological consequences of variations in reaction affinity, using published studies of natural settings as examples.

EQUILIBRIUM PHASE DIAGRAMS AND REACTION AFFINITY

A *P–T* phase diagram section, such as illustrated in Fig. 3a, represents a *P–T* map of phase configurations that give the minimum free energy (G) for the chemical system of interest. The magnitude of the free-energy difference between competing phase configurations for a given *P–T* condition is not apparent on a phase diagram. This energy difference is irrelevant when considering a purely equilibrium system, or a purely

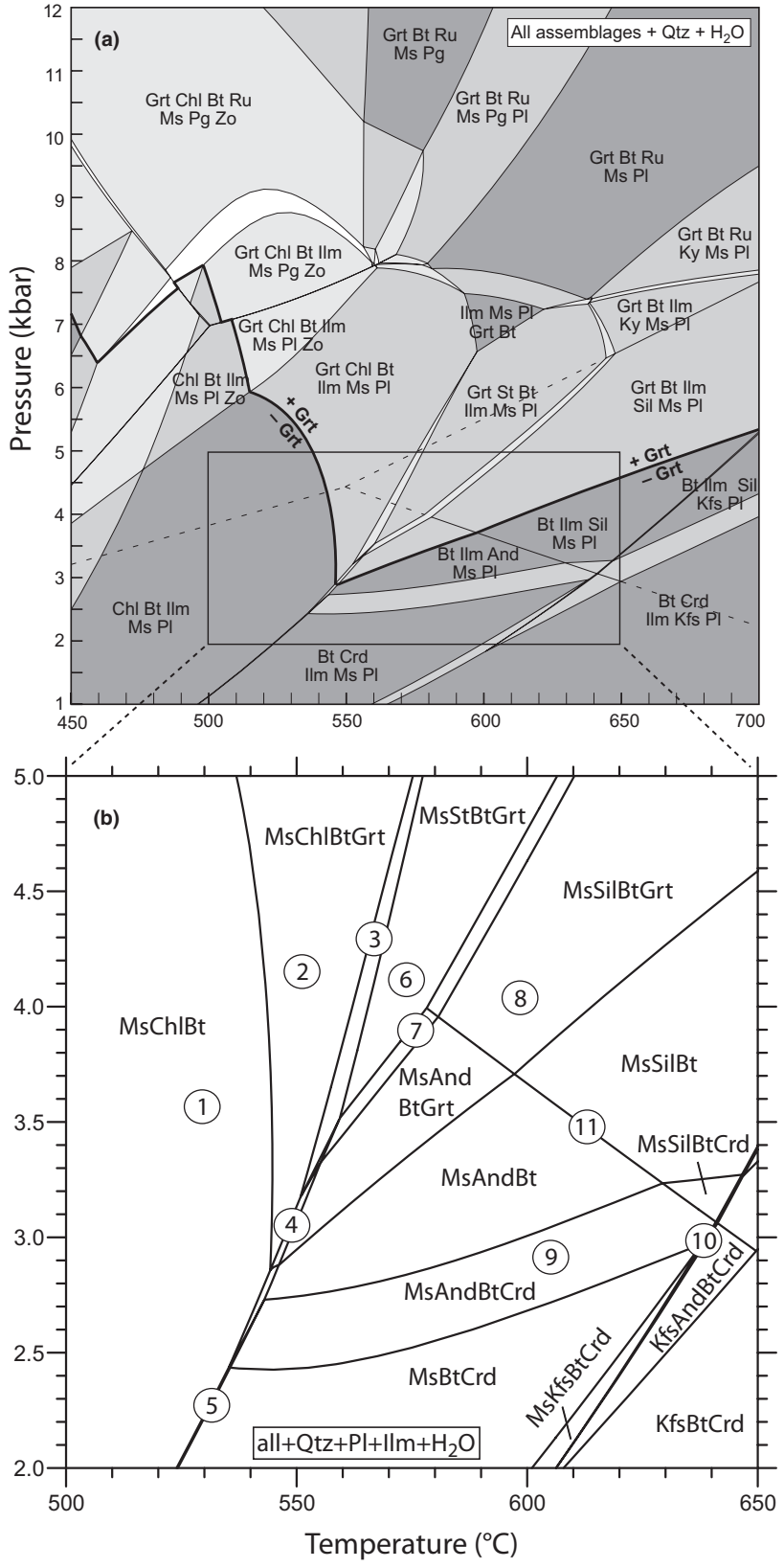

Fig. 3. (a) *P–T* phase diagram section for average Nelson metapelite calculated in the MnNCKFMASHT system (from Pattison & Tinkham, 2009). The bulk composition is given in Table 1. See text for details. (b) Detail of Fig. 3a. This is the base phase diagram for Figs 4–13. Mineral abbreviations from Kretz (1983).

equilibrium approach to natural processes for which the calculated phase diagram is a model, because the minimum free energy is always assumed to be attained regardless of how small the differences between competing phase configurations. In natural processes, however, where any equilibrium boundary must be overstepped to some degree to proceed, or where competing phase configurations might differ only slightly in free energy, this energy difference is potentially important.

The chemical energy that builds up when a reaction boundary is overstepped is the reaction affinity (see Fig. 1). At a certain point, the accumulated chemical energy overcomes the kinetic energetic barriers to nucleation and growth, and reaction proceeds. The free energy of the system drops back down to a lower energy state, possibly (but not necessarily) the lowest energy state (Rubie, 1986, 1998; Fig. 1b,c). Successive traversing of a number of reactions along a prograde P–T path is therefore predicted to result in a broadly sawtooth-type pattern of A *v.* T, such as illustrated in fig. 18b of Pattison & Tinkham (2009) and later in this article.

For overstep in temperature (ΔT), reaction affinity is related to the entropy difference (ΔS) between the stable and metastable states, through the relation:

$$A = \Delta T * \Delta S \quad (2)$$

where $\Delta T = T - T_{eq}$ (Fig. 2). For overstep in pressure (ΔP), reaction affinity is related to the volume difference (ΔV) between these two states, through the relation:

$$A = \Delta P * (-\Delta V) \quad (3)$$

where $\Delta P = P - P_{eq}$. For overstep in composition (ΔX), reaction affinity is expressed by the relation:

$$A = RT * \Delta \ln a \quad (4)$$

where $\Delta \ln a = \ln a - \ln a_{eq}$, with '$a$' related to '$X$' through the relation $a = \gamma X$, where γ is the activity coefficient. Oversteps in composition can arise in any continuous reaction interval in which phases attempt to adjust to equilibrium compositions, but they are especially important in situations involving infiltration of fluids of a different composition from those in equilibrium with the rock. Notwithstanding the importance of infiltration-driven metamorphism in numerous metamorphic settings (e.g. Ferry, 1988, 1991, 1994; Ferry & Gerdes, 1998), in this article we are primarily concerned with overstepping due to temperature and to a lesser degree pressure.

Equation 2 shows that reaction affinity, per unit of temperature overstep, is larger for reactions involving a significant change in entropy, such as devolatilization reactions, than for reactions involving a small entropy change, such as solid–solid reactions. Some examples are given in Table 1 and Fig. 2. For the same energetic threshold for reaction, large-ΔS reactions are predicted to be overstepped less than small ΔS-reactions (Fig. 2). Similar relations pertain to variations in reaction affinity with pressure, the main determinant being magnitude of ΔV. The difference kinetically between a temperature overstep and a pressure overstep is that temperature increase accelerates the kinetic components of reaction, whereas pressure variation has a minor effect (Lasaga, 1998).

Phase diagram for a typical metapelite

Figure 3 shows phase diagram sections for the average composition of metapelite from the Nelson aureole, British Columbia (Pattison & Vogl, 2005). The portion of the phase diagram section between 2 and 5 kbar and 500 and 650 °C (Fig. 3b) is focused on because it involves reactions of varying reaction entropy. The bulk composition of the rock is given in Table 2. In terms of the AFM projection (Thompson, 1957), the average Nelson bulk composition has an A value of 0.1 and an Mg/(Mg + Fe) of 0.46 (following projection from ilmenite and pyrrhotite), close to the average worldwide pelite. The phase equilibria in Fig. 3, and in all subsequent diagrams, are modelled in the chemical system MnNCKFMASHT (MnO–Na_2O–CaO–K_2O–FeO–MgO–Al_2O_3–SiO_2–H_2O–TiO_2, with C and P_2O_5 deleted from the whole-rock analysis, followed by projection from pyrrhotite; see Pattison & Tinkham, 2009, pp. 264–265 for a discussion of choice of chemical system).

The phase diagrams were calculated using the Theriak–Domino phase equilibrium modelling software (de Capitani & Brown, 1987; de Capitani & Petrakakis, 2010). The molar bulk composition used as input to Theriak–Domino is given in Table 2. In the Theriak algorithm, sufficient oxygen is added to the bulk composition to achieve electroneutrality. Fifty moles of hydrogen (equivalent to 25 moles H_2O) were added to the anhydrous bulk composition to ensure that a_{H_2O} was unity across the phase diagram (equivalent to aqueous fluid being available as a possible reactant or product across the diagram). A melt phase was not considered in the modelling because only subsolidus processes are discussed in this article; however, the approach and interpretations below apply equally to melt-bearing situations.

The thermodynamic database used for the calculations is that of Holland & Powell (1998), updated to data set 5.5 in 2003 that incorporates the Al_2SiO_5 triple point of Pattison (1992). Activity models used in all calculations are those used in Tinkham & Ghent (2005) with the following exceptions: (i) margarite was not considered as a component in white mica, and (ii) the ternary feldspar model of Holland & Powell (2003), using a molecular mixing model and asymmetric formalism, was used instead of separate plagioclase and pure orthoclase or sanidine. The choice of database and activity–composition relations is made recognizing that there are some inconsistencies in predicted element

Table 1. Reactions and reaction entropies.

No.	Reaction	End-member KFASH/KMASH reaction	MnNCKFMASHT 'whole-rock' reaction[a]	No. O's in porphyroblast	KFASH/KMASH ΔS^b per O in porphyroblast	ΔS^b per O in porphyroblast	MnNCKFMASHT No. O's in reaction products	ΔS^b per O in reaction
1	Bt-in (from Chl)	None (need solid solutions)	0.41Ms + 0.41Chl + 0.39Pl + 0.3Ilm = 1**Bt** + 1.27Qtz + 1.07H_2O	Bt: 12	n/a	Not calculated	Not calculated	Not calculated
2	Grt-in (from Chl)	0.25Ms + 0.75Chl + 0.75Qtz = 1**Grt** + 0.25Bt + 3H_2O	2.16Ms + 2.50Chl + 1.93Pl + 0.23Ilm = 1**Grt** + 4.66Bt + 5.00Qtz + 7.39H_2O	Grt: 12	16.0	10.3	86.5	1.4
3	St-in (from Chl)	5.1Ms + 3.9Chl = 1**St** + 5.1Bt + 4.1Qtz + 13.5H_2O	7.00Ms + 3.23Chl + 0.23Grt + 0.27Ilm = 1**St** + 5.05Bt + 6.27 Qtz + 1.45Pl + 12.86H_2O	St: 48	16.4	16.8	145.8	5.5
4	And-in (from Chl)	0.63Ms + 0.38Chl = 1**And** + 0.63Bt + 0.13Qtz + 1.5H_2O	0.90Ms + 0.34Chl + 0.03Ilm = 1**And** + 0.64Bt + 0.47Qtz + 0.19Pl + 1.53H_2O	And: 5	18.8	20.5	16.8	6.1
5	Crd-in (from Chl)	1Ms + 1Chl + 2Qtz = 1**Crd** + 1Bt + 3.4H_2O[c]	1.40Ms + 0.93Chl + 1.53Qtz + 0.04Ilm = 1**Crd** + 1.04Bt + 0.28Pl + 4.03H_2O	Crd: 18	15.6	16.5	36.7	8.1
6	Grt to St (Chl-free)	3.9Ms + 5.3Grt + 2.1H_2O = 1**St** + 3.9Bt + 8.2Qtz	11.34Ms + 0.20Ilm + 0.43Grt = 1**St** + 0.10Bt + 10.0Pl + 2.86Qtz + 10.0H_2O	St: 48	−3.7	0.3	145.6	0.1
7	St to And (Chl-free)	0.13Ms + 0.10St + 0.27Qtz = 1**And** + 0.13Bt + 0.19H_2O	0.26Ms + 0.10St + 0.14Qtz + 0.02Ilm = 1**And** + 0.14Bt + 0.09Pl + 0.02Grt + 0.31H_2O	And: 5	3.6	5.0	7.8	3.2
8	Grt to And (Chl- and St-free)	0.5Ms + 0.5Grt = 1**And** + 0.5Bt + 0.5Qtz	1.16Ms + 0.08Grt + 0.04Ilm = 1**And** + 0.18Bt + 0.15Qtz + 0.80Pl + 0.97H_2O	And: 5	0.2	0.9	14.9	0.3
9	And to Crd (Chl-free)	0.25Bt + 1**And** + 0.88Qtz + 0.22H_2O = 0.25Ms + 0.38Crd[c]	0.36Bt + 1**And** + 1.32Qtz + 0.11H_2O = 0.21Ms + 0.46Crd + 0.12Pl + 0.001Ilm	And: 5	2.4	0.3	12.0	0.1
10	And + Kfs-in	1Ms + 1Qtz = 1**And** + 1Kfs + 1H_2O	1.04Ms + 0.85Qtz + 0.001Ilm + 0.12Pl + 0.001Crd = 1**And** + 1.11Kfs + 0.017Bt + 1.02H_2O	And: 5	14.2	12.0	15.1	4.0
11	Sil-in (from And)	1And = 1**Sil**	1And = 1**Sil**	Sil: 5	0.5	0.6	5.0	0.6

[a]Calculated using Theriak–Domino.
[b]J K^{-1}.
[c]Assuming 0.6 moles H_2O pfu in Crd.
Entropies of end-member reactions calculated at 3.5 kbar, 550 °C, except reactions 9 & 10 at 3.5 kbar, 650 °C.
Entropies of MnNCKFMASHT 'whole-rock' reactions calculated using the 'phase exclusion' Method 3 (see text). O, Oxygen. The phases indicated in bold are the ones to which the number of O's in Column 5 refer. They also correspond to the shorthand descriptions of the reactions in Column 2.

partitioning and reaction topology compared to evidence from nature (see discussions in Pattison *et al.*, 2002 and Pattison & Vogl, 2005, p. 73). However, these do not affect the substance of what follows. Discussion of uncertainties in the phase equilibrium modelling is provided in Waters & Lovegrove (2002) and Powell & Holland (2008).

We do not consider non-H_2O fluid species (e.g. C-bearing and S-bearing species), even though they are likely to have been present in some of the rocks under consideration, especially graphitic pelites. In graphitic pelites, in the absence of fluid infiltration, a_{H_2O} in an aqueous fluid is internally buffered to values between ~0.7 and 0.95 for the *P–T* conditions of Fig. 3 (Connolly & Cesare, 1993). This causes modest down-temperature displacements of the dehydration reactions of 5–15 °C (Pattison *et al.*, 2002; Pattison, 2006). We also do not consider the effects of minor elements, in particular zinc which is preferentially fractionated into staurolite, because in the natural staurolite-bearing pelitic schists examined in the second part of the article, and in other 'normal' staurolite-bearing pelitic schists of which we are aware (e.g. Pattison *et al.*, 1999, pp. 696–697), zinc contents of staurolite are modest and do not result in displacements of the Zn-free equilibria by more than 10 °C.

Variations in *G, S, V* and H_2O for a typical metapelite

Figure 4a shows a *P–T* map of the Gibbs free energy of the chemical system listed in Table 2. The phase diagram section of Fig. 3b is superimposed on the free-energy map in Fig. 4b. Despite the significant phase changes across the diagram (from Ms + Chl-rich assemblages typical of greenschist facies phyllites to Kfs + Sil-bearing assemblages typical of upper amphibolite facies gneisses), the smooth *G–P–T* surface shows that the energy differences between these markedly different petrological assemblages are small compared to the total free energy of the system.

Figure 4c shows a *P–T* map of the first derivative of the *G*-surface with respect to temperature (the negative of the total entropy of the system), calculated by finite difference for each pixel as $(G_1–G_2)/(T_1–T_2)$. Figure 4e shows a *P–T* map of the first derivative of the *G*-surface with respect to pressure (the total volume of the system), also calculated by finite difference. In Fig. 4c, the total entropy of the system shows broad

Table 2. Average Nelson whole-rock compositions used for phase diagram modelling.

Raw analysis[a] (wt%)		Raw analysis (mol.%)		MnNCKFM-NASHT[b] (mol.%)		Input for Theriak–Domino (moles)	
SiO_2	60.41	SiO_2	68.53	SiO_2	69.89	Si	100.55
TiO_2	0.93	TiO_2	0.80	TiO_2	0.81	Ti	1.17
Al_2O_3	20.10	Al_2O_3	13.44	Al_2O_3	13.70	Al	39.43
FeO	5.68	FeO	5.39	FeO	5.44	Fe	7.82
MnO	0.08	MnO	0.08	MnO	0.08	Mn	0.12
MgO	2.30	MgO	3.89	MgO	3.96	Mg	5.70
CaO	1.06	CaO	1.29	CaO	1.32	Ca	1.90
Na_2O	1.53	Na_2O	1.68	Na_2O	1.71	Na	4.92
K_2O	4.17	K_2O	3.02	K_2O	3.08	K	8.85
P_2O_5	0.15	P_2O_5	0.07			H	50.00
LOI	3.09	C	1.77				
		S	0.06				
Total	99.51	Total	100.00	Total	100.00		
CO_2	1.14						
SO_3	0.07						
C	0.31						
S	0.027						

[a]Raw analysis from Pattison & Vogl (2005).
[b]MnNCKFMNASHT: omit C and P_2O_5 from raw analysis, project from pyrrhotite, renormalize to 100%.

domains of slowly changing entropy separated by a few discrete breaks across which there are abrupt increases in entropy. Superposition of the phase diagram of Fig. 3b onto the entropy surface (Fig. 4d) reveals a perfect match between intervals of abrupt entropy increase and certain narrow intervals of devolatilization (dehydration) reaction. The connection between entropy change and devolatilization is underscored by a map of the H_2O content of solids (Fig. 4g,h), which shows abrupt decreases coincident with the abrupt increases in entropy.

The two main entropy breaks occur where chlorite + muscovite react to make staurolite, andalusite or cordierite (reactions 3, 4 & 5 in Fig. 4), and where muscovite reacts out in favour of K-feldspar + andalusite/sillimanite (reaction 10). However, other devolatilization reaction intervals, such as the reaction of muscovite + chlorite to form garnet (reaction 2) or the reaction of staurolite to form andalusite (reaction 7), are accompanied by much smaller changes in entropy and volume. Width of reaction interval is not a reliable determinant of entropy change, as is evident from comparing the entropy change across the chlorite-to-staurolite reaction (reaction 3, large entropy change) and staurolite-to-andalusite reaction (reaction 7, small entropy change), both of similar width. Thus, cursory examination of an equilibrium phase diagram may not be sufficient to reveal intervals where entropy change (and therefore the build-up of reaction affinity) is high or low. An additional inherent feature of diagrams like Fig. 4c is that the total-system Gibbs energy, entropy and volume changes are specific to the bulk composition of interest. For example, garnet is a modally minor phase for the bulk composition and P–T range of Fig. 4, so that the effect of garnet growth on the total entropy of the system is minor, even though the entropy change per mole of garnet growth is significant (more below).

CALCULATION OF REACTION AFFINITY

Calculating reaction affinity due to overstepping in natural systems is an inexact exercise because the nature of the compositional departures of reactant and product phases from equilibrium cannot be predicted. Some reactant phases may change composition as the reaction is overstepped whereas others may not, and the composition of product minerals that do finally nucleate and grow are unknown other than within limits. An additional complication is the nature of the rate-limiting mechanism that controls overstepping. Whereas nucleation requires a finite degree of overstepping to proceed, rates of reactant dissolution or intergranular transport increase gradually such that, in situations where these processes are rate limiting, there may be no definite point at which reaction can be considered to initiate.

The approach adopted most commonly (e.g. Walther & Wood, 1984; Lasaga, 1986; Waters & Lovegrove, 2002; Pattison & Tinkham, 2009) involves estimating reaction affinities using simplified end-member reactions that provide an approximation to the more complex reactions that actually proceeded in the rocks. Focusing on temperature overstepping, the equation for reaction affinity becomes $A = \Delta T^* \Delta_r S_{P,T}$, where $\Delta_r S_{P,T}$ is the end-member entropy change of the model reaction at P and T. Table 1 lists stoichiometries (column 3) and entropies (column 6) for a number of simple-system end-member (univariant) reactions, calculated as in Pattison & Tinkham (2009; their table 3). The end-member entropies in Table 1 are normalized per mole of oxygen in the product porphyroblast phase to allow comparison between reactions (Waters & Lovegrove, 2002).

A deficiency in applying the values in Table 1 to the real reactions in the rocks is the effect of multivariancy, in which the compositions of individual minerals change as reaction proceeds (e.g. Fe–Mg exchange). Multivariancy results in reactions proceeding over a temperature interval rather than at a single temperature, as illustrated in the T–$X_{Fe–Mg}$ diagrams of Thompson (1976) for metapelite reactions. Pattison & Tinkham (2009) attempted to simulate this effect in their calculations of reaction affinity by introducing a reaction progress variable across Fe–Mg divariant reactions.

In this study, three different approaches were attempted to obtain estimates of reaction affinity in multicomponent systems that may provide a closer estimate of processes operating in real rocks. All used the Theriak–Domino G-minimization software (de Capitani & Brown, 1987; de Capitani & Petrakakis, 2010). The three methods were tested against reactions 2, 3 and 7 in Table 1. Reaction 2 involves formation of garnet from a muscovite + chlorite matrix (a

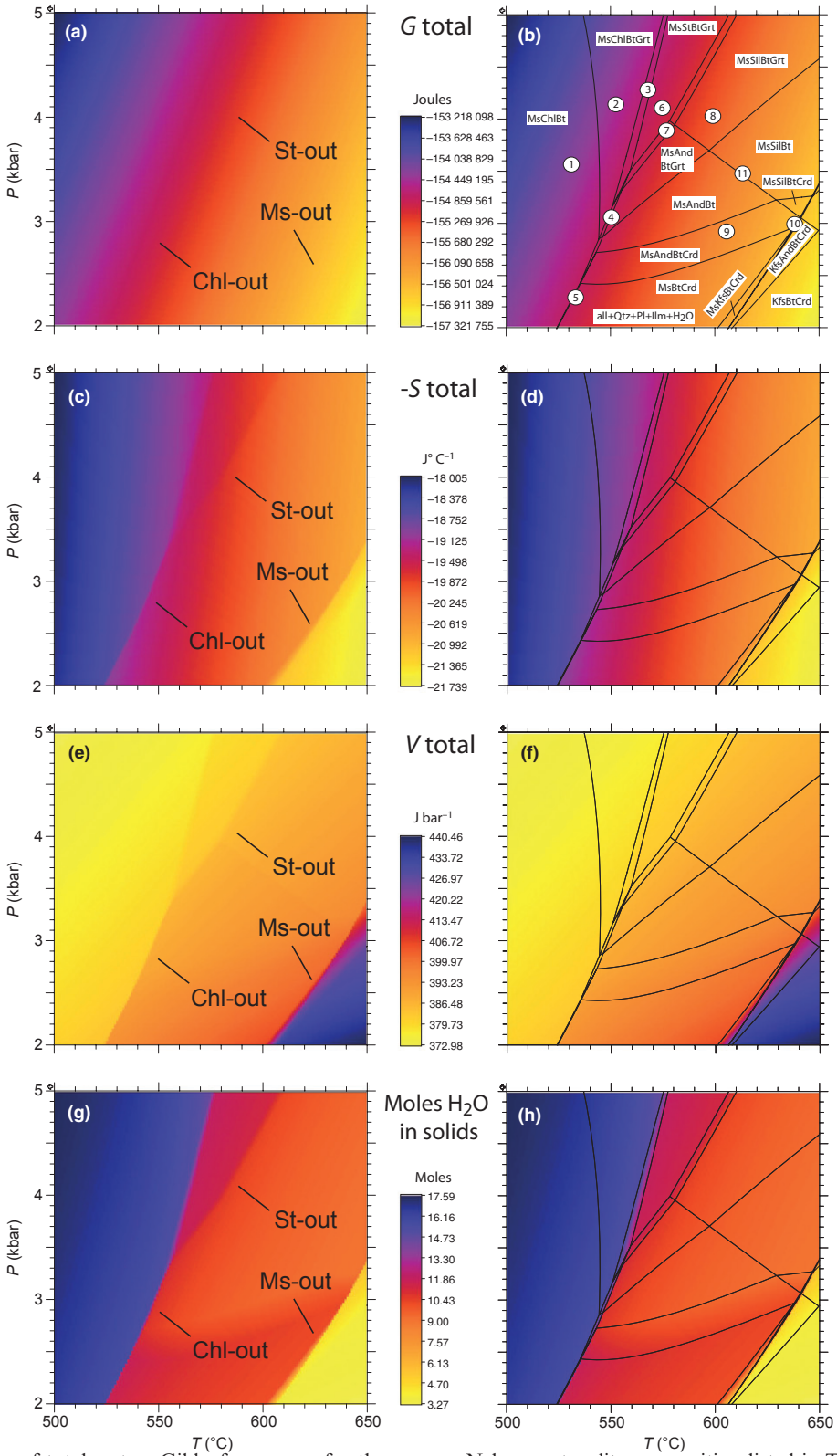

Fig. 4. (a) *P*–*T* map of total-system Gibbs free energy for the average Nelson metapelite composition listed in Table 2. (b) Same as (a), with phase diagram from Fig. 3b superimposed. (c) *P*–*T* map of total-system entropy, average Nelson metapelite. (d) Same as (c), with phase diagram from Fig. 3b superimposed. (e) *P*–*T* map of total-system volume, average Nelson metapelite. (f) Same as (e), with phase diagram from Fig. 3b superimposed. (g) *P*–*T* map of moles of H_2O contained in solid phases, average Nelson metapelite. (h) Same as (g), with phase diagram from Fig. 3b superimposed. All diagrams calculated using the 'pixelmaps' routine of Theriak–Domino (de Capitani & Petrakakis, 2010).

Table 3. Summary of methods to calculate reaction entropy.

Reaction no.	Reaction abbreviation	End-member	Method 1	Method 2	Method 3
2	Grt-in from Chl	16.0	5.1	25	10.3
3	St-in from Chl	16.4	8.2	6–9	16.8
7	And-in from St	3.6	8.3	3–7	5.0

All values in J K^{-1}, normalized per mole of oxygen in the porphyroblast phase of interest (see Table 1).

high-entropy reaction that occurs over a wide multivariant interval, cf. Thompson, 1976). Reaction 3 involves formation of staurolite from a muscovite + chlorite matrix (also a high entropy reaction, but one that occurs over a narrow multivariant interval). Reaction 7 involves formation of andalusite from staurolite + muscovite (a low entropy reaction because the amount of H_2O released is small). The results are listed in Table 3.

Method 1

For the reaction of interest, e.g. formation of garnet by reaction 2, two total free-energy diagrams as in Fig. 4a were calculated: one for the equilibrium assemblage; the second for an equilibrium assemblage in which the porphyroblast of interest, e.g. garnet, was suppressed as a possible phase (hereafter referred to as the 'reactant assemblage'). Up-temperature of the equilibrium garnet-in boundary, the free-energy difference between the two *G*–*T* surfaces in principle should increase with overstep temperature, allowing a direct estimate of the reaction affinity for garnet formation from matrix for any overstep.

This approach is a simplification because two equilibrium states involving different modes and mineral compositions are being compared, which is not the same as comparing a stable and metastable state. What this method models is the failure of the nucleation step, assuming that all other equilibration processes amongst the other phases continue as normal. Some of these processes, including variations in Fe–Mg ratio, tschermak exchange in mica or anorthite content of plagioclase, imply diffusion and intergranular exchange of tightly coordinated cations in response to small energetic driving forces, raising the question as to whether such continous compositional change happens when a reaction is overstepped.

The resultant energy differences were divided by the temperature overstep, and normalized to one oxygen unit in the specified product porphyroblast (Waters & Lovegrove, 2002), allowing comparison with the end-member reaction entropies in Table 1. The difference between the modes of the two states results in a mass balance that approximates the 'whole-rock' reaction involved in the formation of the porphyroblast, subject to the uncertainty noted above. These reactions are listed in Table 1 beside the end-member reactions. Some of the stoichiometries are similar to the end-member reactions, whereas others are quite different. The latter most likely reflect participation of phases in the whole-rock multicomponent reactions that are not involved in the end-member reactions (e.g. mica, plagioclase). The multicomponent reactions in Table 1 may therefore be quite sensitive to the rock bulk composition and to activity–composition models.

Although all three test reactions showed positive entropy changes as expected, the relative magnitudes do not agree with the end-member estimates (Table 3). For example, the highest normalized entropy change was obtained from the chlorite-free, staurolite-to-andalusite reaction 7, even though it is predicted to release less H_2O than the chlorite-consuming reactions 2 and 3. The reasons for this result are uncertain, but might relate to energetic effects arising from compositional changes within modally abundant phases like muscovite and plagioclase in the two equilibrium *G*–*T*–*X* states, and possible changes in the amount of H_2O gained or released associated with these compositional changes.

Method 2

To take account of the possibility that matrix minerals do not equilibrate continuously when a reaction is overstepped, Method 2 considers the other 'end-member', namely that there is no change in mineral compositions when a reaction is overstepped. To this end, Method 1 was modified such that the compositions of the minerals in the 'reactant assemblage' were fixed at their values immediately down-temperature (< 1 °C) of the point of entry of the porphyroblast of interest. The resulting fixed-composition *G*–*T* surface was then subtracted from the equilibrium *G*–*T* surface as described above. The results show unusual trends with temperature (giving rise to the ranges reported in Table 3) and bear little resemblance to the end-member values.

Method 3

The third method attempted takes an entirely different approach, based on Thompson & Spaepen (1983; see also Hillert, 1999, 2008; Hillert & Rettenmayr, 2003). This method was designed to investigate the free energy driving force for nucleation of a phase in systems where compositional variation occurs. The approach is illustrated schematically in Fig. 5 using garnet nucleation from a generic 'matrix', recognizing that a rock matrix in reality comprises numerous phases with individual *G*–*X* surfaces. In Fig. 5a, the garnet-free energy is above the matrix *G*-surface so garnet is not predicted to form. In Fig. 5b the garnet *G*-surface is mutually tangential with the matrix *G*-surface for the bulk composition of interest. This is the equilibrium garnet-in line. In Fig. 5c, the garnet *G*-surface is below the tangent to the matrix *G*-surface for the specified

bulk composition, such that there is an energetic driving force for nucleation. As overstepping increases (Fig. 5d), the free-energy difference between the potential porphyroblast and matrix increases.

To calculate this energy, a modification of the 'Theriak' code was made that excludes garnet from the stable mineral assemblage, yet calculates its molar free energy so that it can be compared with the molar free energy of the garnet-free matrix assemblage. The difference between the two is the molar chemical driving force for nucleation of the garnet. The algorithm to calculate the molar free energy of the garnet is the same as used by 'Theriak' in the search for the minimum-*G* phase configuration of a chemical system, and is described in detail in de Capitani & Brown (1987). In this approach, the relative chemical potentials amongst components in the matrix and in the garnet are the same (the parallel dashed lines in Fig. 5c,d; cf. Thompson & Spaepen, 1983). This gives the maximum possible free-energy difference between garnet and matrix, and therefore is the composition of maximum probability for the formation of a garnet nucleus.

The composition of the garnet nucleus of maximum-*G* difference is not the same as the composition of the garnet that would crystallize if equilibrium were followed, which is the point on the garnet *G*-surface that is mutually tangential with the matrix *G*-surface (solid line in Fig. 5c,d). The difference between the two compositions increases as overstepping increases (Gaidies *et al.*, 2011; Fig. 5c,d). Whether the overstepped garnet that finally nucleates and grows approaches the equilibrium composition is controlled by the efficiency of chemical diffusion through its volume and across its interface with the rock matrix.

Because Method 3 is specific to the nucleation process, the calculated reaction affinity for a given reaction and overstep may not pertain if a different kinetic step is rate limiting. For example, where the reactant and product phases are already present in the rock (e.g. reaction 8: the reaction of muscovite + garnet to andalusite + biotite, upgrade of staurolite consumption), sluggish porphyroblast (garnet) dissolution may be rate limiting. In this situation, Method 3 may give an overestimate of the energy that

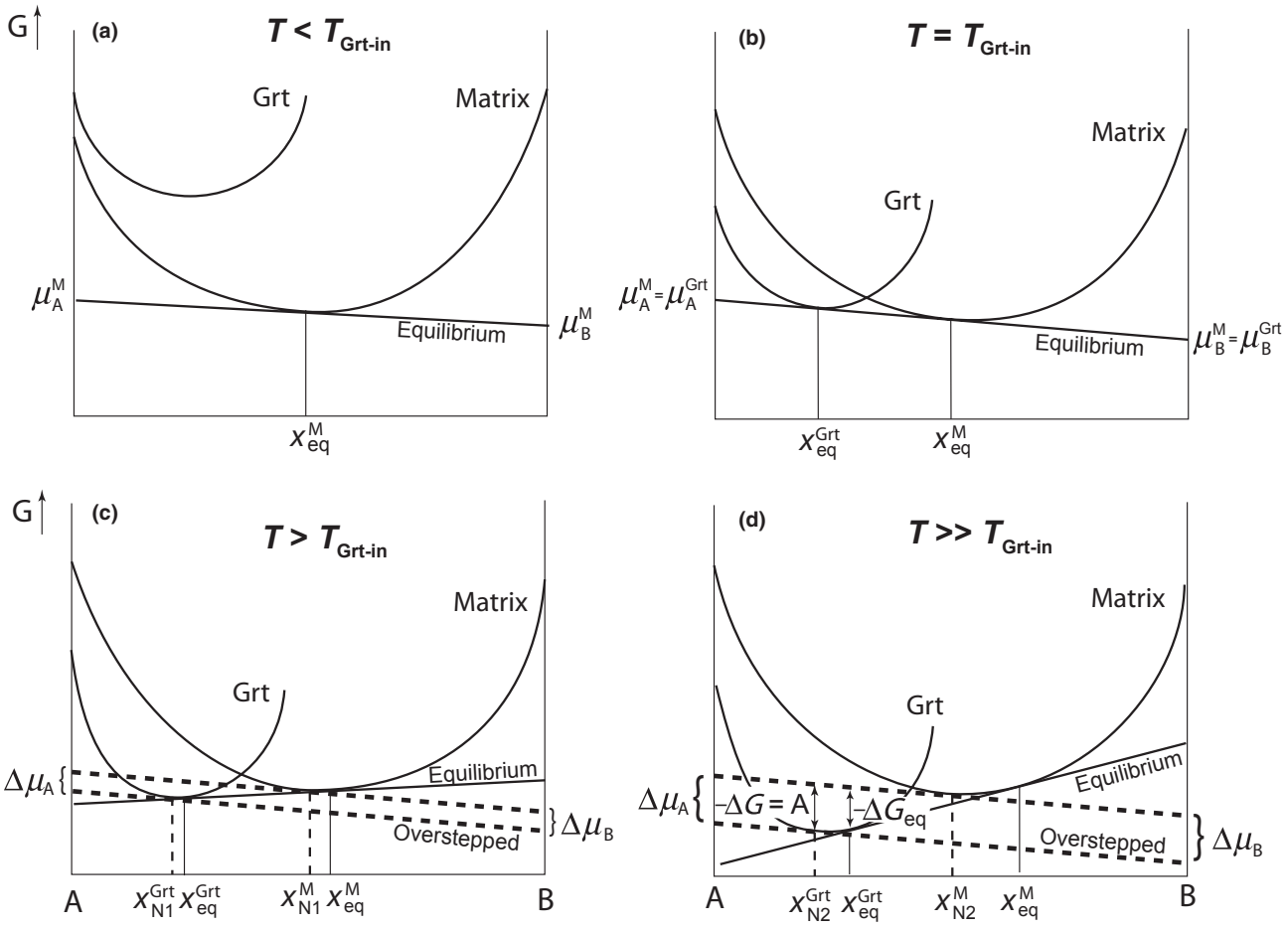

Fig. 5. Schematic free energy–composition (*G*–*X*) diagrams, illustrating the approach used to calculate reaction affinity of formation of a porphyroblast (in this case garnet) from a matrix assemblage. See text for explanation. N1, N2 = composition of overstepped garnet after small and large degrees of overstepping.

builds up with overstepping before reaction proceeds measurably. Such situations are more difficult to model because, as noted earlier, there is no easily definable point at which rates of dissolution, growth or transport increase sufficiently to allow efficient reaction (a possible exception may be the point at which enough intergranular fluid builds up in the grain boundaries to markedly increase rates of dissolution and intergranular transport, as discussed below). Nevertheless, differences in the reaction affinities calculated by Method 3 may flag processes where metastable reactants are more likely to persist.

In summary, while Method 3 may not apply in all situations, it likely provides a maximum estimate of the affinity that builds with overstepping, and a useful measure of relative differences between reactions. Referring to Table 3, the normalized reaction entropies using Method 3 for the three test reactions show a better match with the end-member estimates and the expected effects of multivariancy than Methods 1 and 2. Reaction 2, involving garnet formation from a chlorite + muscovite matrix, has a lower normalized entropy (10 J K^{-1}) than reaction 3, involving staurolite formation from a chlorite + muscovite matrix (16 J K^{-1}), consistent with the greater width of the multivariant interval (esp. Fe–Mg) of the former (cf. Thompson, 1976). Reaction 7, involving andalusite formation from a chlorite-free, staurolite + muscovite matrix, has the lowest normalized entropy (5 J K^{-1}), as expected.

On the basis of this assessment, we proceeded to use Method 3 to assess variations in reaction affinity related to overstepping. An additional advantage of this method over Methods 1 and 2 is that for any P–T condition, the affinity is calculated internally in 'Theriak' and is output directly, without the need to compute and subtract G-surfaces for different reaction intervals. It is therefore ideally suited for the automated calculation of reaction affinity 'maps', as described below.

Normalization

The normalization scheme used above, to one oxygen unit in the product porphyroblast (Waters & Lovegrove, 2002), is specific to the free energy released due to nucleation of a porphyroblast from a matrix assemblage (Thompson & Spaepen, 1983; Hillert, 1999; Waters & Lovegrove, 2002; Gaidies *et al*., 2011). Once nucleation has occurred, or in situations where nucleation is not rate limiting, the processes of dissolution, transport and growth, involving several phases, are involved in the overall reaction and dissipate the chemical energy (reaction affinity) that has built up with overstepping. For this growth stage of reaction, a more relevant normalization scheme for reaction affinity may be with respect to a reaction progress variable (cf. Prigogine & Defay, 1954), or to a molar unit of total product assemblage. As a first approximation, we renormalized the results obtained from Method 3 to one oxygen unit in the multiphase product assemblage using the multicomponent, 'whole-rock', reactions from Method 1, recognizing that Methods 1 and 3 are based on different assumptions and that the stoichiometries of these reactions remain subject to some uncertainty. The results are listed in the last column in Table 1. Although it can be questioned whether renormalizing a nucleation-related reaction affinity to provide information about overall reaction affinity is justified, we again argue that the results likely provide an upper limit and a useful comparative measure between reactions.

The reaction-normalized results show some interesting differences from the porphyroblast-normalized results. For example, garnet formation from a muscovite + chlorite matrix (reaction 2) involves more substantial modal participation of 'matrix' minerals than in staurolite, andalusite or cordierite formation from the same reactants (reactions 3–5), lowering the reaction-normalized reaction entropy of the former compared to the latter. As noted earlier, this reaction stoichiometry may be particular to the Nelson bulk composition, as modelling of garnet formation from a muscovite + chlorite matrix in other bulk compositions gives results closer to the end-member reaction (D. J. Waters, written comm., 2011). The renormalization effect is even greater with Chl-free reactions 6, 8 and 9, resulting in very small normalized reaction entropies that are less than that of the andalusite–sillimanite polymorphic reaction (Table 1).

A significant practical advantage of the porphyroblast normalization scheme is that the number of oxygens in each porphyroblast is a fixed quantity (to a close approximation), in contrast to reactions in which stoichiometry varies from reaction to reaction, and depends upon assumptions about what the 'true' reaction is (e.g. end-member *v*. 'whole-rock' reaction). The porphyroblast normalization scheme is thus especially amenable to automated calculation of reaction affinity maps, recognizing that the calculated affinities may require renormalization if processes other than nucleation are being considered.

REACTION AFFINITY MAPS

Figures 6a–9a show maps of porphyroblast-normalized reaction affinity of formation (strictly nucleation) of garnet, staurolite, andalusite and cordierite relative to a matrix in which these minerals are absent, calculated using Method 3. Affinities were calculated at discrete P–T points in a grid, using the 'pixelmaps' routine of Theriak–Domino (de Capitani & Petrakakis, 2010). Because the maps are based on molar values, they give an indication of reaction affinity independent of how much of the porphyroblast is formed, an advantage compared to what can be inferred from total-system-entropy diagrams like Fig. 4c that depend on modal amounts.

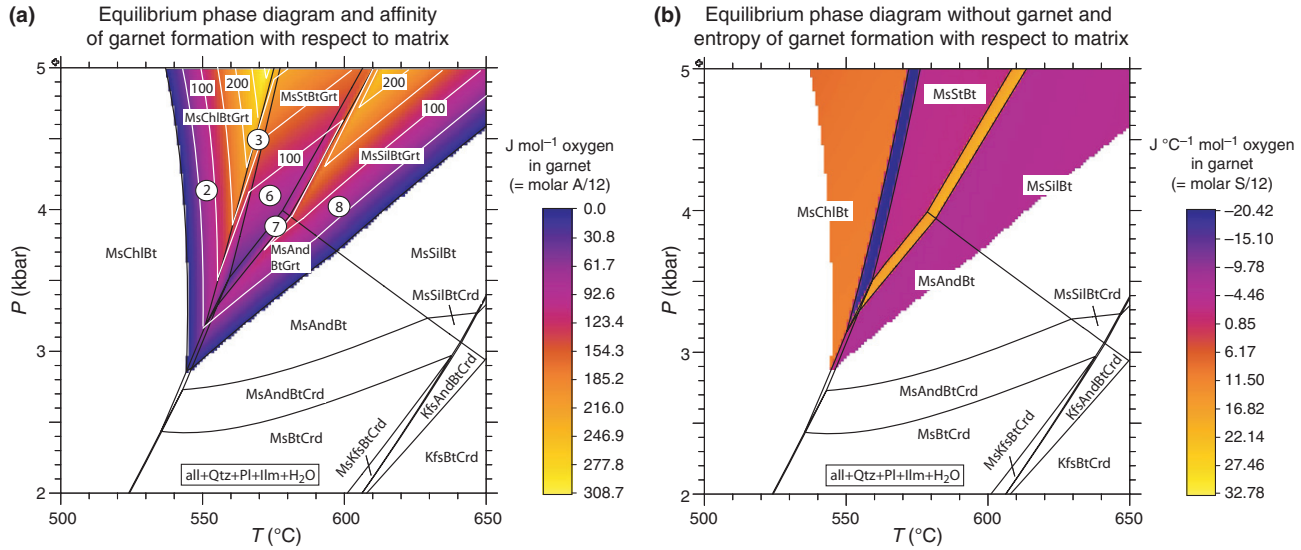

Fig. 6. (a) Reaction affinity of garnet formation relative to a garnet-free matrix assemblage, calculated per mole of oxygen in garnet according to Method 3. Contours are in intervals of 50 J. The phase diagram of Fig. 3b is superimposed. Numbered reaction intervals correspond to the reactions in Table 1. (b) Entropy of garnet formation relative to a garnet-free matrix assemblage, calculated per mole of oxygen in garnet. The *garnet-free* phase diagram is superimposed. See text for explanation. Mineral abbreviations from Kretz (1983).

Superimposed on the reaction affinity maps is the equilibrium phase diagram section from Fig. 3b. Intervals of positive reaction affinity (coloured regions in Figs 6–9) correspond to intervals on the equilibrium phase diagram where the porphyroblast of interest is predicted to be part of the stable mineral assemblage. Changes in trends of reaction affinity (e.g. from increasing to decreasing) correspond to boundaries across which the mineralogy of the *matrix* changes, against which the Gibbs energy of the porphyroblast of interest is being compared.

The mineral assemblage changes *in the matrix* are shown in the phase diagrams in Figs 6b–9b. These were calculated in Theriak–Domino by omitting as a possible phase the porphyroblast of interest (e.g. in Fig. 6b, garnet). The coloured intervals in Figs 6b–9b are the first derivatives with respect to temperature of the reaction affinities in Figs 6a–9a, calculated by finite difference for each pixel as $(G_1–G_2)/(T_1–T_2)$. They provide an estimate of the entropy change associated with the (potential) nucleation of the porphyroblast with respect to the matrix. Positive entropy change indicates intervals where the porphyroblast is predicted to grow relative to the matrix; negative entropy change indicates intervals where the porphyroblast is predicted to be consumed relative to the matrix.

Taking as an example Fig. 6a, reaction affinity of garnet formation increases up-temperature of the garnet-in line where the matrix consists of muscovite + chlorite (reaction 2), but then starts to decrease in the vicinity of, but a little down grade of, reaction 3 where staurolite first appears according to equilibrium. The explanation is provided by Fig. 6b, the garnet-*absent* phase diagram. The garnet-free, staurolite-in reaction takes place a little down grade of the garnet-bearing, staurolite-in reaction in Fig. 6a. Because garnet is predicted to be a reactant phase in staurolite formation, its reaction affinity with respect to the staurolite-bearing matrix therefore drops with increasing temperature. In Fig. 7, the maximum Gibbs energy difference between staurolite and matrix occurs where the matrix assemblage changes from andalusite-free to andalusite-bearing.

Care is therefore required in the preparation and interpretation of the diagrams. A key step is deciding how to treat the matrix mineralogy against which the reaction affinity of the phase of interest is compared. For example, in Fig. 6, if one is interested in the build-up of reaction affinity of garnet relative to matrix over a temperature interval that *crosses a phase change in the matrix assemblage* (e.g. staurolite-forming reaction 3), the reaction affinity up-temperature of the phase change in the matrix may not be meaningful because it implies perfect equilibrium behaviour of the matrix. This includes growth or consumption of porphyroblast phases such as staurolite, an unrealistic assumption when nucleation and growth of these porphyroblasts must themselves be overstepped to some degree.

To avoid this situation, it is possible to suppress staurolite and any other porphyroblast phases that might become stable in the matrix assemblage. Figure 10 illustrates this approach, in which all possible porphyroblast phases (including unexpected phases like corundum and hercynite) were suppressed to allow the desired muscovite–chlorite–biotite reactant assemblage

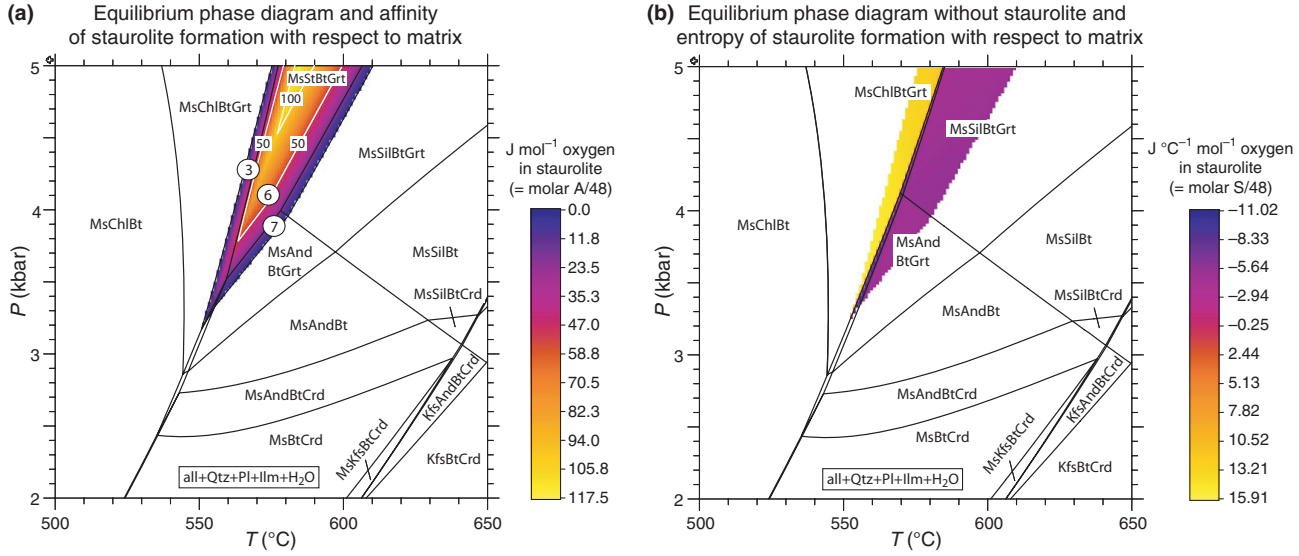

Fig. 7. (a) Reaction affinity of staurolite formation relative to a staurolite-free matrix assemblage, calculated per mole of oxygen in staurolite according to Method 3. Contours are in intervals of 50 J. The phase diagram of Fig. 3b is superimposed. Numbered reaction intervals correspond to the reactions in Table 1. (b) Entropy of staurolite formation relative to a staurolite-free matrix assemblage, calculated per mole of oxygen in staurolite. The *staurolite-free* phase diagram is superimposed. Mineral abbreviations from Kretz (1983).

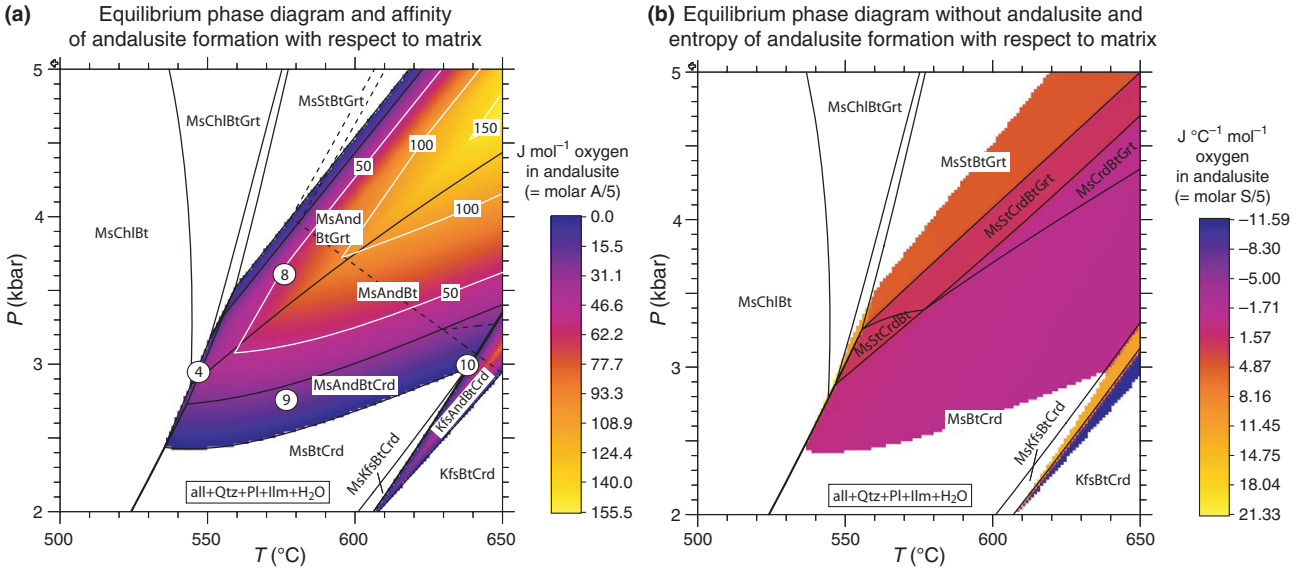

Fig. 8. (a) Reaction affinity of andalusite formation relative to an andalusite + kyanite + sillimanite-free matrix assemblage, calculated per mole of oxygen in andalusite according to Method 3. Contours are in intervals of 50 J. The solid lines of the superimposed phase diagram are the same as Fig. 3b except that reactions involving sillimanite or kyanite have been suppressed (i.e. only reactions involving andalusite are shown); reactions involving kyanite or sillimanite are shown as dashed lines. Numbered reaction intervals correspond to the reactions in Table 1. (b) Entropy of andalusite formation relative to an andalusite + kyanite + sillimanite-free matrix assemblage, calculated per mole of oxygen in andalusite. The *andalusite + kyanite + sillimanite-free* phase diagram is superimposed. See text for explanation. Mineral abbreviations from Kretz (1983).

to persist well up-temperature (Fig. 10b). This allows the build-up of reaction affinity associated with overstepping of garnet formation by reaction 2 (Fig. 10a) to be calculated over a broader temperature interval compared to Fig. 6a. An interesting feature of Fig. 10a is that the entire (equilibrium) multivariant reaction interval of muscovite + chlorite to garnet + biotite, ~40–50 °C wide, is revealed.

In Fig. 8 build-up of reaction affinity associated with nucleation of andalusite from a muscovite + chlorite

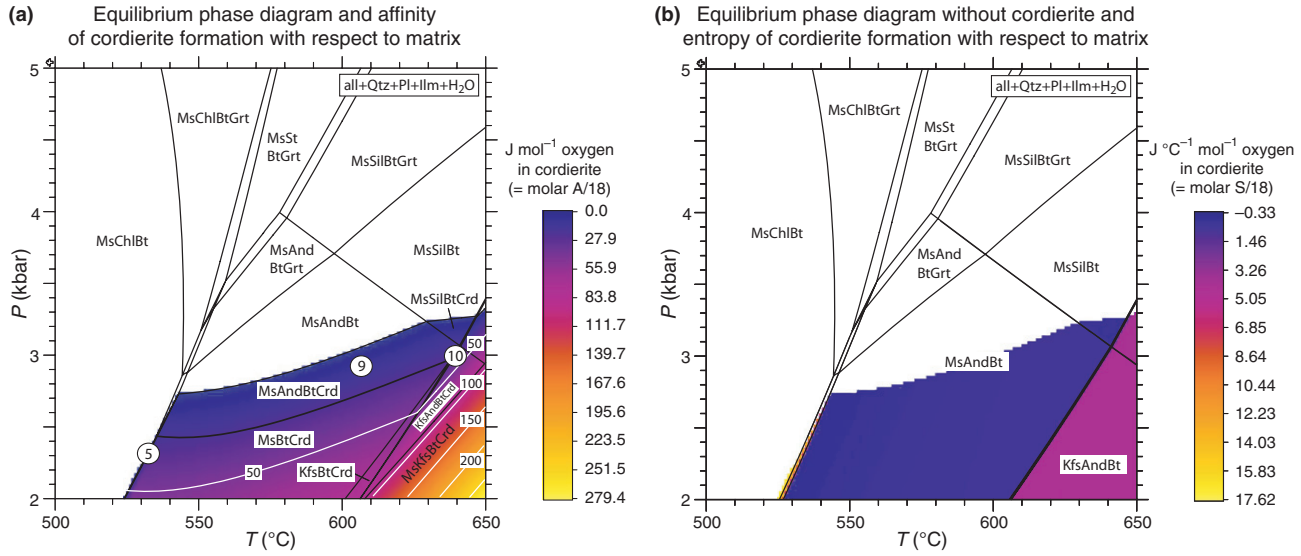

Fig. 9. (a) Reaction affinity of cordierite formation relative to a cordierite-free matrix assemblage, calculated per mole of oxygen in cordierite according to Method 3. Contours are in intervals of 50 J. The phase diagram of Fig. 3b is superimposed. Numbered reaction intervals correspond to the reactions in Table 1. (b) Entropy of cordierite formation relative to a cordierite-free matrix assemblage, calculated per mole of oxygen in cordierite. The *cordierite-free* phase diagram is superimposed. Mineral abbreviations from Kretz (1983).

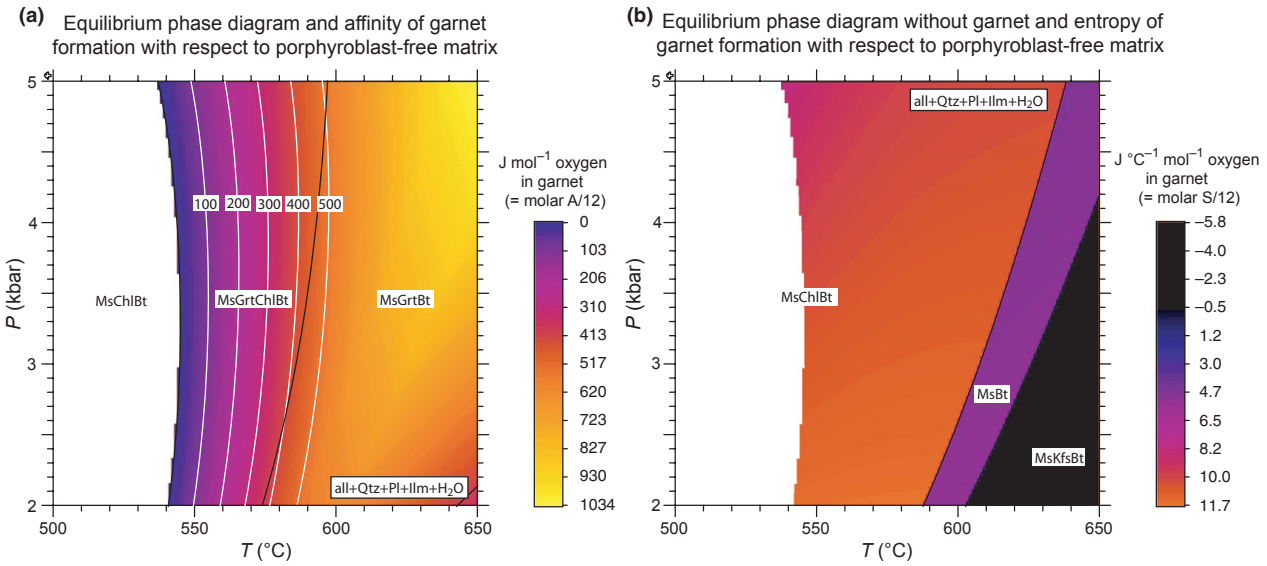

Fig. 10. (a) Reaction affinity of garnet formation relative to a porphyroblast-free matrix assemblage, calculated per mole of oxygen in garnet according to Method 3. The diagram is designed to show build up of reaction affinity for reaction 2 without interference from other porphyroblasts (compare with Fig. 6). Contours intervals of 100 J, up to 500 J, are shown to facilitate comparison with Figs 11 & 12. The superimposed phase diagram shows the stability of garnet relative to the porphyroblast-free matrix. (b) Entropy of garnet formation relative to a porphyroblast-free matrix assemblage, calculated per mole of oxygen in garnet. The *porphyroblast-free* phase diagram (same as in Fig. 11b) is superimposed. Mineral abbreviations from Kretz (1983).

matrix (reaction 4) is difficult to assess because in the andalusite-free matrix, cordierite develops from muscovite + chlorite at similar temperatures as andalusite does, and therefore consumes chlorite over a small temperature interval. Suppression of cordierite and all other possible porphyroblast phases from the matrix allows the build-up of reaction affinity associated with overstepping of reaction 4 to be more clearly seen (see Fig. 11). Comparison of Figs 10 and 11 illustrates the significant difference in rate of build-up of reaction affinity with overstep between garnet and andalusite formation from a muscovite + chlorite matrix.

A final example concerns the chlorite-free reaction of staurolite to andalusite (reaction 7). In Fig. 8, the

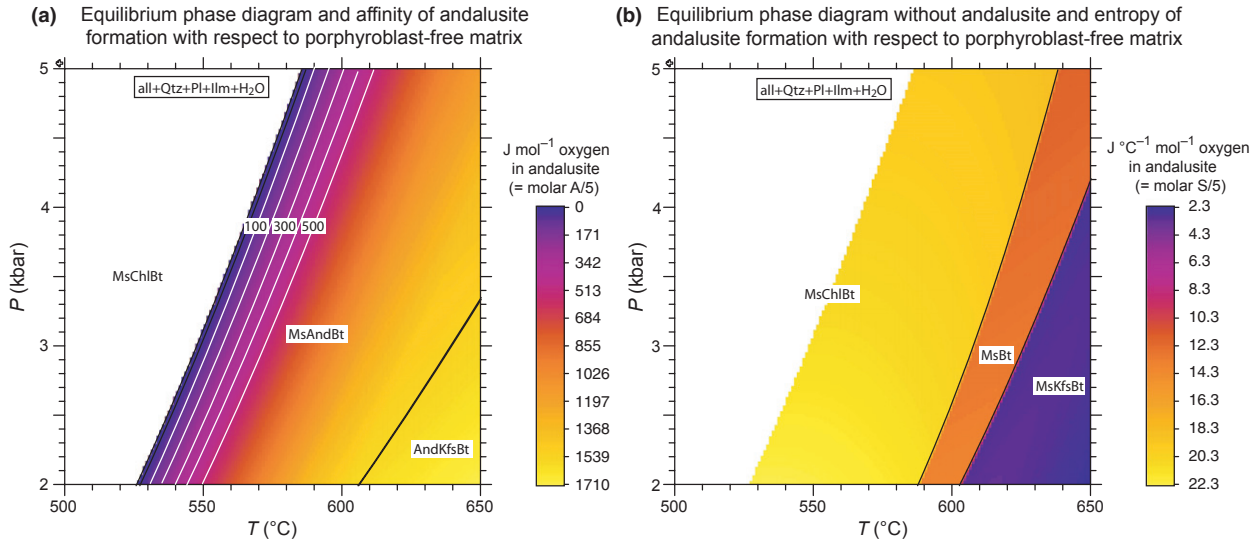

Fig. 11. (a) Reaction affinity of andalusite formation relative to a porphyroblast-free matrix assemblage, calculated per mole of oxygen in andalusite according to Method 3. The diagram is designed to show build up of reaction affinity for reaction 4 without interference from other porphyroblasts (compare with Fig. 8). Contours intervals of 100 J, up to 500 J, are shown to facilitate comparison with Figs 10 and 12. The superimposed phase diagram shows the stability of andalusite relative to the porphyroblast-free matrix. (b) Entropy of andalusite formation relative to a porphyroblast-free matrix assemblage, calculated per mole of oxygen in andalusite. The *porphyroblast-free* phase diagram (same as in Fig. 10b) is superimposed. Mineral abbreviations from Kretz (1983).

build-up of reaction affinity with overstepping of this reaction is partially masked by the substantial domain in which cordierite is predicted to occur in the matrix assemblage. In Fig. 12, cordierite is suppressed, expanding the stability of the staurolite + muscovite assemblage in the matrix against which andalusite is compared energetically, thereby allowing a better assessment of build-up of reaction affinity with overstepping for this reaction. Comparison of Fig. 12 with Figs 10 and 11 illustrates the smaller accumulation of reaction affinity with overstepping for chlorite-free reaction 7 compared to chlorite-consuming reactions 2 and 4.

Applications of reaction affinity maps

We consider reaction affinity maps to be useful in the following situations:

Rapid qualitative evaluation of variations in reaction affinity across a P–T *phase diagram*

Reaction affinity maps such as Figs 6–12 provide a graphic method of assessing in which domains in a *P–T* phase diagram overstepping may be significant, and those in which it may be not. Because the affinities are calculated using Method 3, they pertain to the energy release associated with nucleation, which as discussed above represents maximal affinity for situations where interface or transport processes are rate limiting. In these latter cases, renormalization may be appropriate (see above). An advantage of the reaction affinity maps, compared to calculations of isobaric or isothermal reaction affinity increases like in Table 1, is that variations in reaction affinity for any *P–T* path is easily assessed. Although the focus of this article is on metapelites, the approach can be extended to any chemical system (e.g. metabasites).

The maps show that chlorite-consuming reactions that release substantial H_2O have high entropies and therefore build up reaction affinity markedly with temperature, from which it is predicted that overstepping will be minimal. Broad domains of the phase diagram, upgrade of where chlorite is consumed, show variable and generally more modest changes in reaction affinity, from which it is predicted that overstepping may be more substantial. Reaction affinity involving reaction 9, formation of cordierite from andalusite (or vice versa), builds up especially slowly (Figs 8 & 9), suggesting that reaction involving these minerals may be strongly or even primarily influenced by kinetic factors, or may not occur at all.

Comparison of rate of increase in reaction affinity per unit of overstep for different reactions

An example of where this comparison is useful is the observed large degree of overstepping of the chloritoid-to-staurolite reaction compared to that for the chlorite-to-staurolite reaction in the Bushveld aureole (Waters & Lovegrove, 2002), and the similarly large observed degree of overstepping of the staurolite-to-andalusite reaction compared to that for the chlorite-to-staurolite reaction in the Nelson aureole

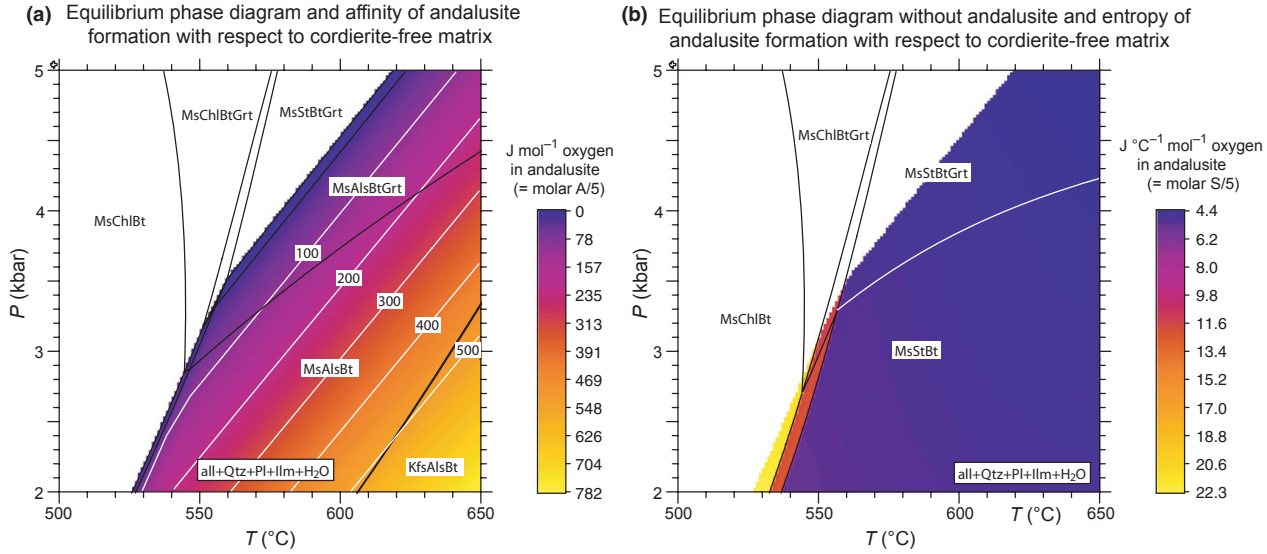

Fig. 12. (a) Reaction affinity of andalusite formation relative to a cordierite-free matrix assemblage, calculated per mole of oxygen in andalusite according to Method 3. The diagram is designed to show build up of reaction affinity for reaction 7 without interference from cordierite (compare with Fig. 8). Contours intervals of 100 J, up to 500 J, are shown to facilitate comparison with Figs 10 and 11. The superimposed phase diagram shows the stability of andalusite relative to the cordierite-free matrix. (b) Entropy of andalusite formation relative to a cordierite-free matrix assemblage, calculated per mole of oxygen in andalusite. The *cordierite-free* phase diagram is superimposed. Mineral abbreviations from Kretz (1983).

(Pattison & Tinkham, 2009). In these examples, difficulty of nucleation was considered to be the rate-limiting step. The differences can be accounted for by the different relative rates of build-up of reaction affinity with overstep for chlorite-consuming reactions (rapid) compared to chlorite-free reactions (slow).

Comparison of rate of increase in reaction affinity per unit of overstep for different porphyroblasts growing from the same reactants

An example where this comparison is useful is the greater observed overstepping of garnet formation from a muscovite + chlorite-rich matrix in the Nelson aureole relative to staurolite formation from the same matrix assemblage (more details below). Comparison of Figs 7 and 10 shows that the entropy change, and therefore rate of build-up of reaction affinity with overstep, is greater for garnet than for staurolite, consistent with the observations.

Fractionation effects

One potentially important factor that is not taken into account in the calculation of the reaction affinity maps is the effect of prograde fractionation associated with porphyroblast growth. With respect to an individual reaction, fractionation will not affect the nucleation step of a reaction, but will substantially affect the dissolution and growth steps by changing the reactive bulk composition and therefore the chemical driving force (affinity) for continued reaction (Waters, 1990; Gaidies *et al.*, 2011). With respect to the reaction affinity maps, change in the reactive bulk composition arising from prograde fractionation changes the *P–T* position of mineral stability fields and mineral compositions compared to the non-fractionation case, sometimes dramatically (e.g. Evans, 2004). For example, in their study of the Nelson aureole, Pattison & Tinkham (2009, p. 273) found that prograde garnet fractionation in the garnet zone impoverished the bulk composition in Fe and especially Mn to the point that no garnet growth was possible upgrade of the development of staurolite, in contrast to Fig. 6. A full exploration of the effects of fractionation *v.* non-fractionation on reaction affinity is beyond the scope of this article.

PETROLOGICAL CONSEQUENCES OF VARIATIONS IN REACTION AFFINITY

The remainder of the article explores some of the petrological consequences of variations in reaction affinity, drawing on examples from the literature. A central question is the degree to which variable reaction affinity compromises the notion of continuous reaction implied in an equilibrium treatment of metamorphism.

Discrete rather than continuous metamorphic reaction intervals that may not correspond with equilibrium boundaries

To evaluate the relative amount of overstepping to be expected amongst different reactions, consider an arbitrary, uniform energetic threshold for any reaction

to proceed, recognizing that in reality such a threshold will vary with porphyroblast, temperature and heating rate, among other factors. In Fig. 2, this threshold is shown as the dotted horizontal line at 300 J mol^{-1} (normalized to one mole of oxygen in the porphyroblast). This value is chosen because it provides a good fit to the estimated overstepping in the Nelson aureole (see below) and is comparable to the estimates of Waters & Lovegrove (2002) for the nucleation of cordierite (~200 J mol^{-1}), staurolite (~400 J mol^{-1}) and andalusite (~1000 J mol^{-1}) in the Bushveld aureole, and the ~170 J mol^{-1} estimate of Wilbur & Ague (2006) for growth of dendritic garnet in the garnet zone of the Connecticut Barrovian metamorphic sequence derived from Monte Carlo simulation (taking their ~2 kJ mol^{-1} per garnet estimate and normalizing it to one mole of oxygen in garnet).

Referring to Fig. 2, the 300 J mol^{-1} oxygen energetic threshold will be reached after ~30 °C overstep for the formation of garnet from muscovite + chlorite (Fig. 10), ~15 °C for the formation of andalusite from muscovite + chlorite (Fig. 11), ~60 °C for the formation of andalusite from staurolite + muscovite (Fig. 12), and not at all for the formation of cordierite from andalusite (Figs 8 & 9). The implication is that, in situations where nucleation is rate limiting, the reaction progress a rock experiences as it traverses different domains on a phase diagram may be less than predicted thermodynamically, is unlikely to be continuous, and where reaction affinity builds slowly, may not occur at all. Reaction is predicted to occur instead in discrete intervals, corresponding to the point at which sufficient reaction affinity has built up to overcome kinetic barriers to nucleation. The smallest overstepping is predicted to be for the reactions with the largest entropy or volume changes. These inferences may extend qualitatively to situations where porphyroblast dissolution or intergranular transport rather than nucleation are rate limiting, recognizing that the point at which reaction is considered to 'go' in these situations is less easily defined and that the absolute values in the affinity maps would require renormalization. Some natural examples are provided below.

Contact metamorphic examples

Nelson aureole, southeastern British Columbia. Figure 13 shows the prograde path of metamorphism in Area D of the Nelson aureole (Pattison & Vogl, 2005; Pattison & Tinkham, 2009) on an equilibrium phase diagram and on accompanying *G–T* and *A–T* diagrams, the latter two schematic to allow the inferred relationships to be more clearly shown. There are three discrete intervals of reaction in this sector of the Nelson aureole, from lowest to highest grade (see fig. 1 of Pattison & Tinkham, 2009): (i) a narrow (~50 m wide) interval ~1300 m from the contact where chlorite reacts out of the fine grained muscovite + chlorite-rich host rock to variably form porphyroblasts of garnet, staurolite and more rarely andalusite; (ii) a narrow (< 50 m wide) interval ~400 m from the contact where staurolite volumetrically breaks down to sillimanite (and subsidiary garnet, the latter based on chemical zoning profiles of garnet); and (iii) a less well constrained interval ~100 m from the contact where muscovite disappears in favour of sillimanite + K-feldspar.

The inferred conditions of the first two reaction intervals are shown on Fig. 13. The *chlorite-out reaction* commences ~30 °C up-temperature of where it is predicted to commence with the formation of garnet. This temperature interval is greater than the ~15 °C interval shown in Fig. 13 because the bulk composition of the average Nelson metapelite used to calculate Fig. 13 is Fe + Mn poorer than the rocks from the garnet zone in Area D (Pattison & Tinkham, 2009, p. 265; Gaidies *et al.*, 2011). Garnet formation occurs close spatially, and therefore close in temperature, to the chlorite-to-staurolite and chlorite-to-andalusite reactions. The *staurolite-out reaction* to sillimanite and garnet occurs ~60 °C upgrade of where it is predicted to occur, in a domain where garnet is predicted to be unstable.

Referring to Fig. 13b,c, there were therefore two main intervals in which reaction affinity built up in a metastable mineral assemblage: first, in the regional chlorite + muscovite assemblage leading up to chlorite breakdown to make garnet, staurolite and less commonly andalusite; and second, in the Al_2SiO_5-absent, staurolite + muscovite assemblage leading up to staurolite breakdown to sillimanite. In both cases, the overstepping was related to difficulty of nucleation, perhaps augmented in the second case by sluggish staurolite dissolution (Pattison & Tinkham, 2009). The order of overstepping (~60 °C for staurolite breakdown, ~30 °C for garnet formation, and no apparent overstepping for staurolite and andalusite formation from chlorite) is consistent with the predictions of Figs 7 and 10–12. If the staurolite-forming and andalusite-forming reactions were themselves overstepped, the estimate for overstepping of garnet formation correspondingly increases, and that for reaction of staurolite to andalusite correspondingly decreases. The key point is that there is no evidence for continuous equilibration and reaction; the evidence indicates instead discrete, overstepped, episodic reaction that, in the case of the staurolite-out reaction, involved metastable reaction unrelated in P–T space to any equilibrium boundary.

Bushveld aureole, South Africa. The sequence of reactions experienced by aluminous pelites in the Bushveld aureole (Waters & Lovegrove, 2002) bears no resemblance whatsoever to the predicted equilibrium sequence, even though the final mineral assemblage is close to that predicted by the equilibrium phase diagram (compare figs 5 & 7 of Waters & Lovegrove, 2002). Reaction of chloritoid was overstepped by some 80 °C, most likely due to a combi-

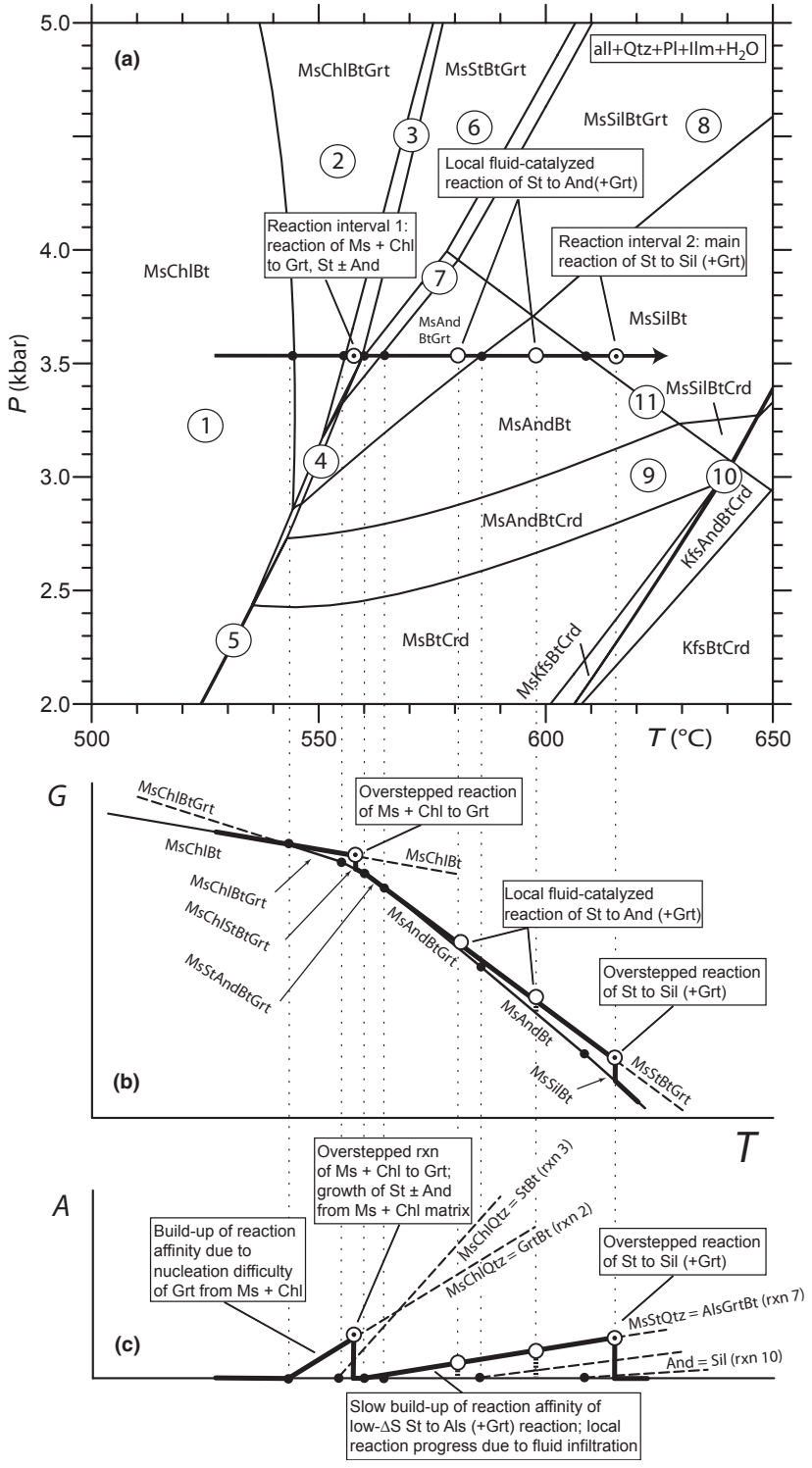

Fig. 13. Prograde reaction evolution in the Nelson aureole, based on Pattison & Tinkham (2009). (a) *P–T* phase equilibrium diagram for average Nelson metapelite (the same as Fig. 3b). Small solid dots on the 3500 bar isobaric *P–T* path are intersections with reaction boundaries on the equilibrium phase diagram, where minerals are predicted to be either gained or lost from the mineral assemblage. Open circles with dots inside are the two main reaction intervals observed in the aureole. Open circles without dots represent localized reaction related to fluid infiltration (see text for explanation). (b) Schematic free energy–temperature (*G–T*) diagram, showing the interpreted prograde evolution at Nelson. The ideal equilibrium path follows the minimum-*G* line segments (solid lines), with breaks in slope occurring at the reaction boundaries (solid dots). Dashed lines represent the metastable *G–T* extensions of select mineral associations. Most of the prograde path in the aureole (bold line) tracks along two of the metastable *G–T* segments (MsChlBt and MsGrtStBt, respectively), dropping back down to the equilibrium *P–T* path once the overstepped reactions proceeded (to make garnet and sillimanite, respectively). (c) Schematic reaction affinity–temperature (*A–T*) diagram for Nelson, showing how reaction affinity rises in intervals of reaction overstepping, and then abruptly drops back down towards zero reaction affinity (equilibrium) once reaction starts and the built-up chemical energy is released. A prograde path crossing several reactions thus shows a sawtooth pattern, with the height of each 'tooth' reflecting the degree of overstepping required before reaction commences. Mineral abbreviations from Kretz (1983).

nation of the low affinity of the chloritoid-consuming reaction, difficulty of nucleation of staurolite, and sluggish dissolution of the chloritoid porphyroblasts (see fig. 9 of Waters & Lovegrove, 2002). Reaction did not proceed until high entropy, chlorite-consuming reactions commenced to produce staurolite and andalusite, at which point several reactions, including the overstepped chloritoid-consuming reactions, proceeded in parallel in a small temperature interval to produce these two minerals.

Bugaboo aureole, southeastern British Columbia. In the Bugaboo aureole (DeBuhr, 1999; Pattison *et al*., 2002), there is an extensive zone of cordierite + andalusite-bearing rocks (Fig. 14). Within a range of co-existing Mg/(Mg + Fe) compositions, there is no significant grade-related variation of cordierite and biotite compositions (Fig. 14a), although the two minerals track each other (i.e. more Mg-rich cordierite co-exists with more Mg-rich biotite). The only significant compositional correlation, out of many examined, is with bulk-rock Mg/(Mg + Fe) (Fig. 14b). The implication is that the minerals attained their compositions when they initially grew from high-entropy chlorite-breakdown reactions (reactions 4 & 5), and did not change thereafter. This pattern is consistent with the very low reaction affinity of the cordierite-to-andalusite reaction (Figs 8 & 9).

Skaergaard aureole, Greenland. In contrast to the above examples, the Skaergaard aureole is developed in basaltic protoliths. Manning *et al*. (1993) reported an abrupt jump from chlorite + actinolite-bearing mineral assemblages in the outer aureole to pyroxene hornfelses in the inner aureole, with no intervening hornblende zone. They attributed the absence of a hornblende zone to nucleation difficulty of hornblende in combination with the low entropy of the hornblende-forming reaction from the anhydrous basaltic protolith, the latter leading to a slow increase in reaction affinity with overstep. The result was that the hornblende-forming reaction was overtaken in reaction affinity by the more strongly H_2O-releasing pyroxene-producing reaction after ~80 °C of temperature overstep.

Other contact metamorphic examples. Buick *et al*. (2004) reported metastable melting of a low grade precursor assemblage in the immediate contact zone of the Rustenburg Layered Suite of the Bushveld Complex, South Africa. This may be an example of particularly rapid heating adjacent to a hot magma, a situation taken to the extreme in the narrow baked zones adjacent to mafic dykes. Muller *et al*. (2004) reported metastable prograde mineral reactions in metacarbonates of the Ubehebe Peak contact aureole. In metacarbonates, fluid is usually an essential reactant (e.g. for the formation of hydrous phases like tremolite). The extent of reaction therefore depends on the timing and efficiency of fluid infiltration as well as on temperature overstepping, a more complex situation to evaluate.

Regional metamorphic examples

Snow Peak Barrovian sequence, Idaho. A regional example that resembles the Nelson aureole example is the carefully documented Barrovian prograde sequence in the Snow Peak area, Idaho (Lang & Rice, 1985a,b,c). Going upgrade from the lowest grade chlorite + biotite zone is a ~2.5 km wide garnet zone, a 4–7 km wide staurolite zone, a 2.5–4 km wide staurolite + kyanite zone, and finally a 1 km wide staurolite-free kyanite zone (fig. 1 of Lang & Rice, 1985c). Of particular note is the wide zone in which staurolite-only and staurolite + kyanite-bearing mineral assemblages occur. Lang & Rice (1985c) documented the Mg/(Mg + Fe) of coexisting ferromagnesian minerals (chlorite, biotite, garnet, staurolite) going upgrade through the sequence (their fig. 13), and compared the variation with predictions from phase equilibrium modelling (their figs 4–16). The latter predicted that the ferromagnesian minerals would change in Mg/(Mg + Fe) going through the

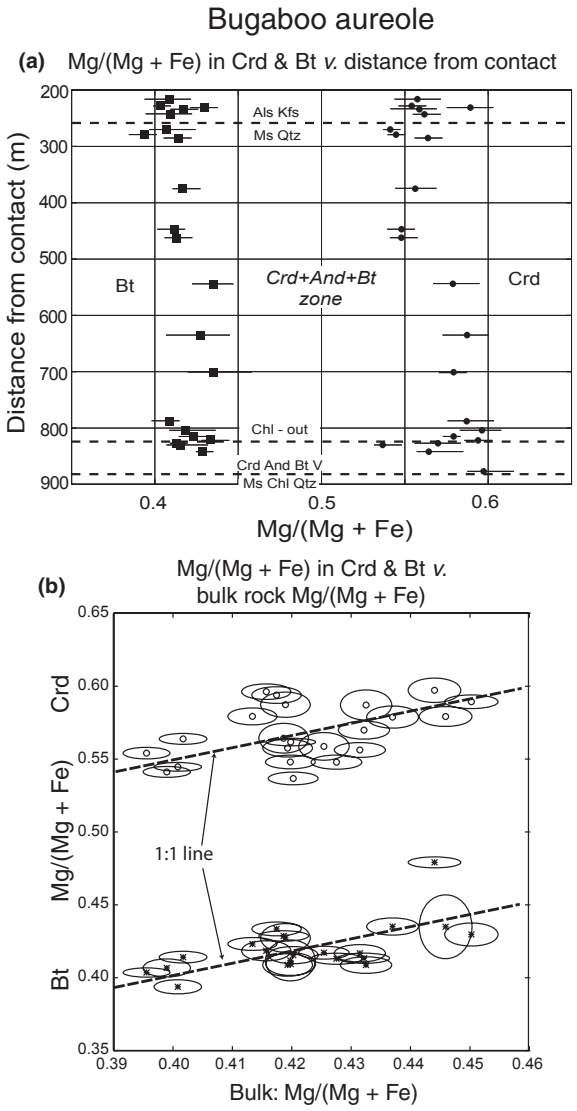

Fig. 14. (a) Trend of Mg/(Mg + Fe) in coexisting cordierite and biotite *v*. distance from igneous contact in the Bugaboo aureole, SE British Columbia (DeBuhr, 1999; Pattison *et al*., 2002). Star symbols – biotite. Dots – cordierite. Bars represent the range of measured analyses. (b) Plot of Mg/(Mg + Fe) in coexisting cordierite and biotite *v*. whole rock Mg/(Mg + Fe) (DeBuhr, 1999). 1:1 trend lines have been added by eye.

Fe–Mg divariant reactions, becoming Mg-richer in the staurolite-forming reaction interval and Fe-richer in the kyanite-forming interval. In contrast, the observed compositions show virtually no compositional change going upgrade (staurolite shows none; biotite and garnet show scattered values with a weak trend to Mg-enrichment, independent of mineral assemblage). A possible interpretation is that staurolite and garnet largely attained their compositions when they grew from high-*A* chlorite-consuming reactions, and changed little thereafter because of a combination of low driving force for reaction and sluggish equilibration of the reactant porphyroblasts. The large zone of co-existence of staurolite-only and staurolite–kyanite assemblages, in which staurolite shows no compositional variation, argues for kinetic control on the staurolite-consuming reaction like that inferred in the Nelson aureole.

Other regional examples. Zeh & Holness (2003) estimated overstepping of ~80 °C for garnet nucleation and growth in the regional low-pressure Ilesha belt, Nigeria. This extreme degree of overstepping can be explained by the Al + Mn-rich composition of the samples examined, resulting in predicted initial garnet growth at much lower temperature than for 'ordinary' pelites such as in Fig. 3. Wilbur & Ague (2006) examined garnet showing striking textural sector zoning from the Acadian Barrovian regional metamorphic sequence in Connecticut, and used Monte Carlo simulations of crystal growth to argue for nucleation-related overstepping of the garnet reaction.

Discrete rather than continuous fluid generation and presence

If reaction is episodic rather than continuous, fluid generation, and possibly fluid presence in general, is likewise predicted to be episodic rather than continuous (cf. Thompson, 1983). This may especially be the case where nucleation difficulty leads to significant overstepping, resulting in a discrete period of vigorous reaction and fluid release once the nucleation barrier is overcome. An important additional factor related to fluid presence or absence is its role as a catalyst to reaction (see Introduction).

The Nelson aureole provides evidence for both the catalysing effects of fluid, and the episodicity of fluid generation and presence (Pattison & Tinkham, 2009). Concerning the catalysing effect of fluid, in the staurolite–andausite zone of the aureole (see their fig. 1), there is a wide interval on the ground in which staurolite + andalusite and staurolite-only mineral assemblages occur adjacent to each other at all scales. Figure 3 of their paper shows photomicrographs of the patchy, domainal pseudomorphing of staurolite by andalusite within a single thin section. In the absence of compositional variations, these features are most plausibly explained by the local ingress of fluid. Fluid may have lowered activation energy barriers to reaction, most likely a combination of sluggish staurolite dissolution, difficulty of andalusite nucleation and possibly slow intergranular mass transport. Potential sources of an infiltrating fluid include the dehydrating pelitic rock volume and the nearby intrusion.

An alternative interpretation is that fluid may have acted as a chemical driver if the infiltrating fluid had a significantly reduced a_{H_2O}, below that of the ambient graphite-H_2O buffer in these graphitic rocks (cf. Connolly & Cesare, 1993; Pattison, 2006). A fluid of such low a_{H_2O} would most likely have to be generated from carbonate-bearing rocks, which are minor to absent in this part of the aureole. We therefore prefer a kinetic explanation for this widespread, local phenomenon because the catalytic effect of fluid is largely independent of its composition.

Concerning episodicity of fluid presence, local fluid-catalysed reaction in this part of the aureole implies that the large volume of andalusite-free, staurolite-bearing rock was rendered metastable by virtue of being fluid undersaturated (using the terminology of Carlson, 2010). This implies in turn that the large volume of fluid generated earlier in the history of the rock, in association with chlorite consumption to make staurolite, must have escaped the rock. Thus, both fluid generation and fluid presence were episodic and transitory. Once the kinetic barriers to the staurolite-to-andalusite/sillimanite reaction were overcome in the rocks not affected by fluid infiltration, there may have been another discrete, vigorous pulse of fluid release. Similar speculations about episodic fluid release and presence can be made in the other examples described in the previous section.

Abrupt mineral isograds

Overstepping related to slowly building reaction affinity in multivariant reaction intervals may provide an explanation for the commonly abrupt development in the field of certain index mineral isograds, for example the Barrovian garnet isograd (D. J. Waters, written comm., 2011). The visibility of this isograd in the field may be reinforced by a discrete, kinetically controlled interval of rapid reaction and fluid release in what is otherwise a broad multivariant field (Figs 6 & 10). The abrupt staurolite-out/sillimanite-in isograd in the Nelson aureole may be another example.

Textural features of garnet from the garnet zone of a number of regional settings (e.g. Wilbur & Ague, 2006) and contact settings (e.g. Pattison & Tinkham, 2009) suggests rapid growth, consistent with overstepping. Waters (1990) performed calculations suggesting that rapid porphyroblast growth associated with overstepping of multivariant reactions could condense the nucleation interval, resulting in relatively unimodal crystal size distributions such as found in some regionally metamorphosed rocks. Rapid growth associated with overstepping could also account for

reduced compositional variability compared to equilibrium growth (Waters, 1990), perhaps explaining the narrow compositional range of garnet and other minerals observed by Lang & Rice (1985a,b,c) in their study of the Snow Peak Barrovian sequence.

Cascade effects

Reaction overstepping can result in multiple reactions being energetically possible, both stable and metastable. The only criterion that has to be satisfied is that each possible reaction lowers the free energy of the system. Reaction overstepping can therefore lead to a 'cascade effect', in which several stable and metastable reactions involving the same reactant phases proceed simultaneously in a small temperature interval.

Two different types of cascade effect related to reaction overstepping have been described in the literature. In the Bushveld aureole (Waters & Lovegrove, 2002), a cascade effect developed when the low-entropy chloritoid to staurolite/andalusite reactions were overstepped to the point that they were overtaken in terms of reaction affinity by high-entropy muscovite + chlorite-consuming reactions. Nucleation of staurolite and andalusite by the latter reactions eliminated the principal kinetic barrier to the progress of the overstepped chloritoid-consuming reactions, such that several staurolite-producing and andalusite-producing reactions ran approximately in parallel. Fluid release accompanying reaction may also have contributed to the cascade effect by facilitating dissolution of chloritoid.

The Bushveld aureole provides a good example of the operation of Ostwald's step rule, which states that of several possible reactions, the one that is kinetically most favourable will dominate, rather than the one leading to the lowest free energy. Microtextural evidence shows that cordierite nucleated and grew out-of-sequence before andalusite. Waters & Lovegrove (2002) attributed this to the greater ease of nucleation of cordierite compared to andalusite, related in turn to the lower interfacial energy of cordierite compared to andalusite (Waters, 1990).

In the Nelson aureole, a different type of cascade effect was interpreted to have developed when the overstepped chlorite to garnet reaction initiated, releasing fluid into the grain boundary network (Pattison & Tinkham, 2009). This fluid may have enhanced rates of intergranular transport, facilitating further reaction and fluid release, thereby creating a positive feedback and a vigorous reaction interval. The clustering in the field of the garnet, staurolite and andalusite isograds, and the textural evidence that each of these porphyroblasts, formed from reaction of the matrix with no evidence of consumption of the earlier-formed porphyroblasts as predicted by equilibrium thermodynamics, suggests the simultaneous operation of several chlorite-consuming reactions.

In summary, the first type of cascade (Bushveld type) arises from delayed nucleation of a product phase and subsequent production of that product phase from several different reactants. The second type of cascade (Nelson type) involves a catalytic trigger related to the build-up or influx of fluid, and subsequent production of different product phases from the same reactant minerals.

Interpretation of *P–T* paths from reaction textures

The possibility for metastable reactions, even in situations in which the final mineral assemblage approaches what is predicted from equilibrium thermodynamics, highlights the potential for misinterpretation of *P–T* paths when textures suggesting a particular sequence of mineral growth and consumption are interpreted solely with respect to reactions in an equilibrium phase diagram (cf. Vernon & Powell, 1976; Vernon *et al.*, 2008).

For example, Fig. 15a,b shows samples from the regional low-pressure Buchan sequence near Banff, Scotland, in which andalusite has grown between two cordierite porphyroblasts. Rocks downgrade contain chlorite-free cordierite-bearing mineral assemblages. Assuming a gentle negative slope (Pattison *et al.*, 2002) for reaction 9, the cordierite-to-andalusite reaction (in contrast to the gentle positive slope shown in Figs 3–12), conventional interpretation of this texture with reference to an equilibrium phase diagram suggested sequential passage through reaction 5, the chlorite-to-cordierite reaction (to make cordierite), and reaction 9 (to make andalusite; Hudson, 1980; Pattison *et al.*, 2002). However, examining Fig. 15a,b, there is little evidence of significant cordierite consumption accompanying andalusite development, nor is there any elsewhere in the thin section. Combined with the very low energetic driving force for reaction 9 (Figs 8 & 9), an alternative interpretation is that both minerals grew from a precursor chlorite-bearing matrix at about the same *P–T* conditions, with cordierite growing before andalusite because its growth was kinetically favoured (cf. Waters & Lovegrove, 2002). In contrast, the andalusite–cordierite texture in Fig. 15c from the Bugaboo aureole is more suggestive of sequential passage through the chlorite-to-cordierite and cordierite-to-andalusite reactions because there is evidence for replacement of the cordierite by andalusite.

The *P–T* path of the Bushveld pelites, involving the sequential growth of staurolite, cordierite and andalusite (all with biotite), is even more convoluted if interpreted solely in terms of the equilibrium phase diagram. This sequence would require an abrupt isothermal decrease in pressure from conditions of staurolite growth to conditions of cordierite growth, followed by near-isothermal pressure increase to form andalusite (see fig. 3b and Pattison *et al.*, 1999).

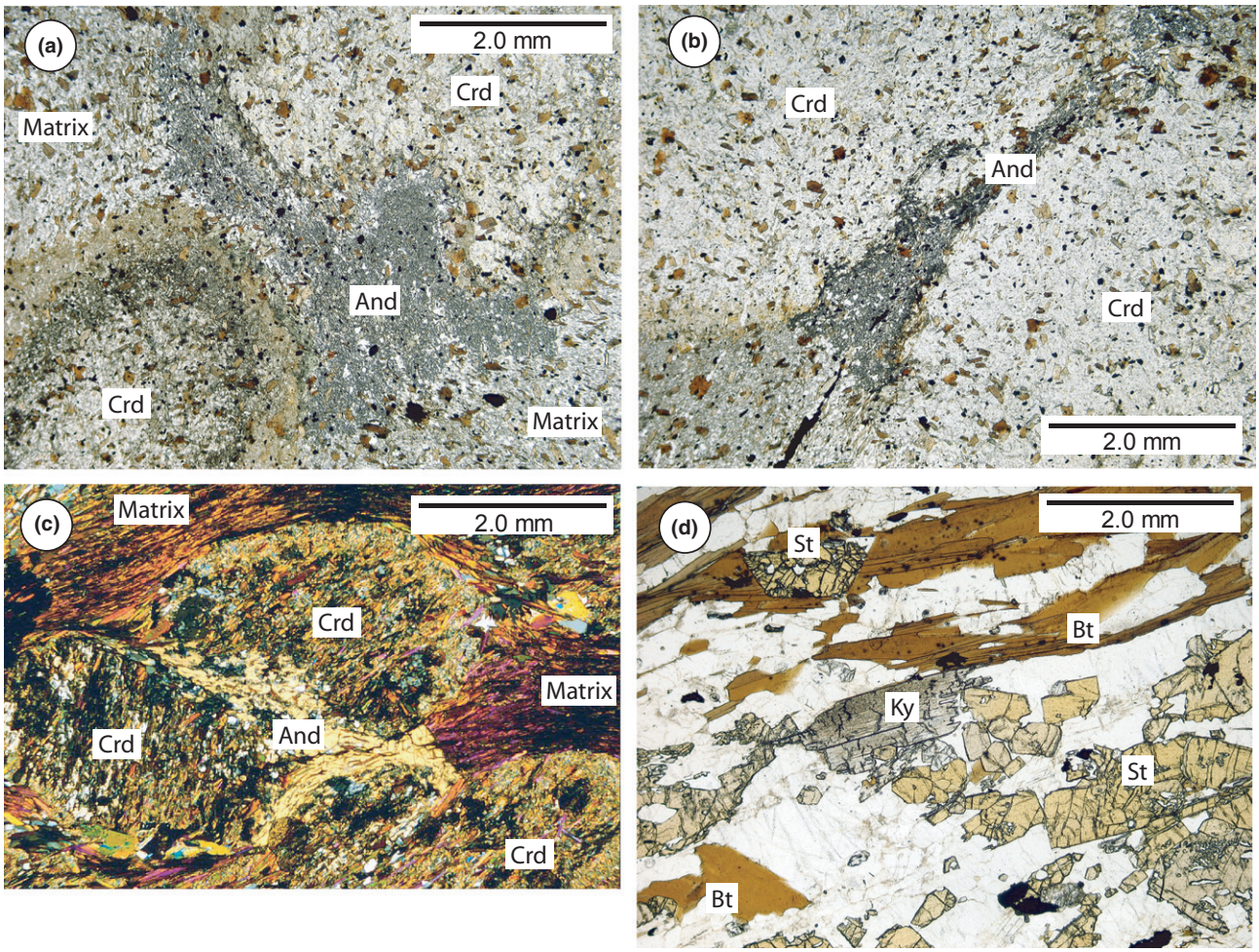

Fig. 15. (a,b) Andalusite growing in between cordierite poikiloblasts, Banff, Scotland. (c) Andalusite growing in between, and partially replacing, cordierite poikiloblasts, Bugaboo aureole, SE British Columbia. (d) Kyanite and staurolite porphyroblasts in schist from the Caplongue aureole, France. Note the absence of any indication of staurolite instability relative to kyanite.

Thermobarometry

In estimating peak *P–T* conditions of metamorphism, the possibility of overstepped and metastable reactions introduces a note of caution to the recommended practice (Powell & Holland, 2008) of combining (i) mineral assemblage domains, mineral modes and mineral compositions in equilibrium phase diagram sections, and (ii) multi-equilibrium thermobarometry. The underlying rationale for this approach, based on the attainment of local equilibrium, is that all should agree within the uncertainty of the thermodynamic data.

In the Nelson aureole, it is predicted that the phase equilibrium and thermobarometry approaches should not agree because some of the minerals (e.g. garnet and staurolite) occur outside of their stability field and, in the case of garnet rims in the andalusite and sillimanite zones, grew metastably. Assuming the composition of the metastably formed garnet rims in the sillimanite zone reflects the *P–T* conditions under which they formed, the thermobarometry results should indicate ~30 °C higher temperature than the phase equilibrium constraints. A test of this prediction was inconclusive because the temperature difference lies within the uncertainty limits of the thermobarometry.

Waters (2010) studied a sillimanite schist from Mt Everest in which he argued, based on microtextures and garnet chemical zoning, that garnet grew only under garnet zone conditions, failed to contribute to staurolite growth, and experienced corrosion under sillimanite conditions without re-equilibrations at its rims. In this case, estimating peak *P–T* conditions by multi-equilibrium thermobarometry using the full mineral assemblage necessarily fails. These two examples do not undermine the rationale for the combined approach advocated by Powell & Holland (2008), but they illustrate the care needed in applying it where

overstepping or other kinetically controlled processes may have affected the mineral assemblage and compositions.

Extrapolation to regional metamorphism: the role of enhanced deformation

Notwithstanding the few regional examples provided above, an important question is whether reaction overstepping is expected to be more common in contact metamorphic settings compared to regional metamorphism. Conventional wisdom suggests that because the time-scales of regional metamorphism, and therefore heating rates, are in general slower than for contact metamorphism, overstepping is expected to be less. Waters & Lovegrove (2002), however, noted that according to classical, steady-state nucleation rate laws, the activation energy for nucleation depends inversely on the square of the temperature overstep, in contrast to other thermally activated processes (e.g. transport, dissolution) whose activation energies are functions of absolute temperature but not of temperature overstep. The result is a sharp increase in nucleation rate over a very small temperature interval (a few degrees), and therefore a small dependence on heating rate (see also Ridley & Thompson, 1986, p. 159). Gaidies *et al.* (2011), in their nucleation simulations, arrived at the same conclusion.

A more significant factor may be the presence or absence of rock deformation occurring during metamorphism (Bell & Hayward, 1991; Waters & Lovegrove, 2002). Deformation assists nucleation by building up strain energy in the reactant phases, contributing to the energy needed to overcome activation energy barriers, and by providing energetically favourable sites for nucleation. Deformation accompanying metamorphism is generally thought to be more common in regional metamorphism compared to contact metamorphism, even though a number of contact aureoles show textures and structures indicative of deformation prior to and during metamorphism (e.g. Fig. 15c from the Bugaboo aureole). The commonly significant width of garnet zones downgrade of the staurolite isograd in regional settings, in contrast to the near-coincident garnet and staurolite isograds in the Nelson aureole, may reflect the enhanced effects of deformation in the former. On the other hand, the fairly common occurrence of simultaneous 'staurolite + andalusite' and 'staurolite + kyanite' isograds in regional metamorphic settings, such as in Augusta, Maine (Osberg, 1968; Ferry, 1980), Snow Peak (Lang & Rice, 1985a,b,c) and Mica Creek, British Columbia (Ghent, 1975), and the common lack of evidence of instability of staurolite in kyanite-bearing rocks, such as illustrated in the photomicrograph from the Caplongue aureole in Fig. 15d, suggest that kinetically related phenomena in regional metamorphism may also occur.

Metamorphic facies

To conclude this article, it was noted in the Introduction that the metamorphic facies principle provides the essential justification for an equilibrium view of metamorphism. The regularity and repeatability of mineral assemblage sequences in contact as well as regional settings (Pattison & Tracy, 1991) suggests that the principle extends to all but the most rapidly heated contact settings. It is therefore interesting to pose the question whether kinetically controlled phenomena such as described above represent violations of the metamorphic facies principle.

The results of this article suggest that metamorphic facies boundaries (e.g. greenschist–amphibolite) and the important metamorphic zonal boundaries (e.g. staurolite isograd) correspond to major mineralogical and textural changes that accompany high entropy, H_2O-releasing reactions that consume a dominant hydrous phase such as chlorite, muscovite and, at higher grade, biotite and possibly hornblende (e.g. Fig. 4c). Overstepping is expected to be minimal in such situations, or at least not sufficiently large to disrupt the observed repeatable patterns. It may be that it is mainly, and in some cases perhaps only, in these relatively discrete intervals that significant reaction, fluid release (fluid presence?), recrystallization and chemical equilibration occur. Reaction within domains (facies) between the boundaries may occur, but possibly only discretely at conditions that may bear little correspondence to equilibrium conditions, being controlled as much by the rate of build-up of reaction affinity and the specific kinetic factors of each situation. From this perspective, we find no contradiction between the overall success of the equilibrium approach to metamorphism, as represented by the metamorphic facies, and situations in which kinetics have influenced metamorphic reaction progress. Although the broad features of a metamorphic sequence may be accounted for by an equilibrium model, the details of isograd patterns, mineral textures, and mineral composition and chemical zoning, likely require consideration of both equilibrium and kinetics.

ACKNOWLEDGEMENTS

We thank J. Ague, J. Ferry and D. Waters for their helpful reviews which led to improvements in the content and clarity of the paper. D. Waters contributed particularly incisive insights throughout the course of this research. This research was supported by NSERC Discovery Grant 037233 to Pattison.

REFERENCES

Austrheim, H., 1987. Eclogitization of lower crustal granulites by fluid migration through shear zones. *Earth and Planetary Science Letters*, **81,** 221–232.

Bell, T.H. & Hayward, N., 1991. Episodic metamorphic reactions during orogenesis – the control of deformation partitioning on reaction sites and reaction duration. *Journal of Metamorphic Geology*, **9,** 619–640.

Buick, I.S., Stevens, G. & Gibson, R.L., 2004. The role of water retention in the anatexis of metapelites in the Bushveld Complex aureole, South Africa: an experimental study. *Journal of Petrology*, **45,** 1777–1797.

de Capitani, C. & Brown, T.H., 1987. The computation of chemical equilibria in complex systems containing non-ideal solutions. *Geochimica et Cosmochimica Acta*, **51,** 2639–2652.

de Capitani, C. & Petrakakis, K., 2010. The computation of equilibrium assemblage diagrams with Theriak/Domino software. *American Mineralogist*, **95,** 1006–1016.

Carlson, W.D., 2010. Dependence of reaction kinetics on H_2O activity as inferred from rates of intergranular diffusion of aluminum. *Journal of Metamorphic Geology*, **28,** 735–752.

Connolly, J.A.D. & Cesare, B., 1993. C-O-H-S fluid compositions and oxygen fugacity in graphitic metapelites. *Journal of Metamorphic Geology*, **11,** 379–388.

DeBuhr, C.L., 1999. *Metamorphic Petrology and Mass Balance Analysis in the Bugaboo Contact Aureole*. Doctoral Thesis, University of Calgary, Calgary, AB, Canada.

de Donder, T., 1922. Affinity. *Bulletin of the Royal Academy of Belgium (Cl. Sc.)* **7,** 197, 205. Available at: http://en.wikipedia.org/wiki/Chemical_thermodynamics.

de Donder, T., 1936. *Thermodynamic Theory of Affinity: A Book of Principles*. Oxford University Press, Oxford.

Eskola, P., 1915. On the relation between chemical and mineralogical composition in the metamorphic rocks in the Orijarvi region. *Bulletin de la Commission Geologique de Finlande*, **44,** 167–225.

Evans, T.P., 2004. A method for calculating effective bulk composition modification due to crystal fractionation in garnet-bearing schist; implications for isopleth thermobarometry. *Journal of Metamorphic Geology*, **22,** 547–557.

Ferry, J.M., 1980. A comparative study of geothermometers and geobarometers in pelitic schists from south-central Maine. *American Mineralogist*, **65,** 720–732.

Ferry, J.M., 1988. Infiltration-driven metamorphism in northern New England, USA. *Journal of Petrology*, **29,** 1121–1159.

Ferry, J.M., 1991. Dehydration and decarbonation reactions as a record of fluid infiltration. In: *Contact Metamorphism* (ed. Kerrick, D.M.), *Mineralogical Society of America Reviews in Mineralogy*, **26,** 351–394.

Ferry, J.M., 1994. Role of fluid flow in the contact metamorphism of siliceous dolomitic limestones. *American Mineralogist*, **79,** 719–736.

Ferry, J.M. & Gerdes, M.L., 1998. Chemically reactive fluid flow during metamorphism. *Annual Review of Earth and Planetary Science*, **26,** 255–287.

Gaidies, F., Pattison, D.R.M. & de Capitani, C., 2011. Towards a quantitative model of metamorphic nucleation and growth. *Contributions to Mineralogy and Petrology*. DOI 10.1007/s00410-011-0635-2.

Ghent, E.D., 1975. Temperature, pressure and mixed volatile equilibria attending metamorphism of staurolite-kyanite-bearing assemblages, Esplanade Range, British Columbia. *Geological Society of America Bulletin*, **86,** 1654–1660.

Guiraud, M., Powell, R. & Rebay, G., 2001. H_2O in metamorphism and unexpected behavior in the preservation of metamorphic mineral assemblages. *Journal of Metamorphic Geology*, **19,** 445–454.

Hillert, M., 1999. Solute drag, solute trapping and diffusional dissipation of Gibbs energy. *Acta Materialia*, **47,** 4481–4505.

Hillert, M., 2008. *Phase Equilibria, Phase Diagrams and Phase Transformations: Their Thermodynamic Basis*, 2nd edn. Cambridge University Press, Cambridge.

Hillert, M. & Rettenmayr, M., 2003. Deviation from local equilibrium at migrating phase interfaces. *Acta Materialia*, **51,** 2803–2809.

Holland, T.J.B. & Powell, R., 1998. An internally consistent thermodynamic data set for phases of petrological interest. *Journal of Metamorphic Geology*, **16,** 309–344.

Holland, T.J.B. & Powell, R., 2003. Activity-composition relations for phases in petrological calculations: an asymmetric multicomponent formulation. *Contributions to Mineralogy and Petrology*, **145,** 492–501.

Hudson, N.F.C., 1980. Regional metamorphism of some Dalradian pelites in the Buchan area, northeast Scotland. *Contributions to Mineralogy and Petrology*, **73,** 39–51.

Kretz, R., 1983. Symbols for rock-forming minerals. *American Mineralogist*, **68,** 277–279.

Lang, H.M. & Rice, J.M., 1985a. Metamorphism of pelitic rocks in the Snow Peak area, northern Idaho: sequence of events and regional implications. *Bulletin of the Geological Society of America*, **96,** 731–736.

Lang, H.M. & Rice, J.M., 1985b. Regression modelling of metamorphic reactions in metapelites, Snow Peak, Northern Idaho. *Journal of Petrology*, **26,** 857–887.

Lang, H.M. & Rice, J.M., 1985c. Geothermometry, geobarometry and T-X(Fe-Mg) relations in metapelites, Snow Peak, Northern Idaho. *Journal of Petrology*, **26,** 889–924.

Lasaga, A.C., 1986. Metamorphic reaction rate laws and development of isograds. *Mineralogical Magazine*, **50,** 359–373.

Lasaga, A.C., 1998. *Kinetic Theory in the Earth Sciences*. Princeton University Press, Princeton.

Lasaga, A.C. & Rye, D.M., 1993. Fluid flow and chemical reactions in metamorphic systems. *American Journal of Science*, **293,** 361–404.

Manning, C.E., Ingebrisen, S.E. & Bird, D.K., 1993. Missing mineral zones in contact metamorphosed basalts. *American Journal of Science*, **293,** 894–938.

Muller, T., Baumgartner, L.P., Foster, C.T. & Vennemann, T.W., 2004. Metastable prograde mineral reactions in contact aureoles. *Geology*, **32,** 821–824.

Osberg, P.H., 1968. Stratigraphy, structural geology, and metamorphism of the Waterville-Vassalboro area, Maine. *Maine Geological Survey Bulletin*, **20,** 64 pp.

Pattison, D.R.M., 1992. Stability of andalusite and sillimanite and the Al_2SiO_5 triple point: constraints from the Ballachulish aureole, Scotland. *Journal of Geology*, **100,** 423–446.

Pattison, D.R.M., 2006. The fate of graphite in prograde metamorphism of pelites: an example from the Ballachulish aureole, Scotland. *Lithos*, **88,** 85–99.

Pattison, D.R.M. & Tinkham, D.T., 2009. Interplay between equilibrium and kinetics in prograde metamorphism of pelites: an example from the Nelson aureole, British Columbia. *Journal of Metamorphic Geology*, **27,** 249–279.

Pattison, D.R.M. & Tracy, R.J., 1991. Phase equilibria and thermobarometry of metapelites. In: *Contact Metamorphism* (ed. Kerrick, D.M.), *Mineralogical Society of America Reviews in Mineralogy*, **26,** 105–206.

Pattison, D.R.M. & Vogl, J.J., 2005. Contrasting sequences of metapelitic mineral-assemblages in the aureole of the tilted Nelson Batholith, British Columbia: implications for phase equilibria and pressure determination in andalusite-sillimanite type settings. *Canadian Mineralogist*, **43,** 51–88.

Pattison, D.R.M., Spear, F.S. & Cheney, J.Y., 1999. Polymetamorphic origin of muscovite + cordierite + staurolite + biotite assemblages: implications for the metapelitic petrogenetic grid and for P-T paths. *Journal of Metamorphic Geology*, **17,** 685–703.

Pattison, D.R.M., Spear, F.S., BeBuhr, C.L., Cheney, J.T. & Guidotti, C.V., 2002. Thermodynamic modelling of the reaction Muscovite + Cordierite = Al_2SiO_5 + Biotite + Quartz + H_2O: constraints from natural assemblages and implications for the metapelitic petrogenetic grid. *Journal of Metamorphic Geology*, **20,** 99–118.

Powell, R. & Holland, T.J.B., 2008. On thermobarometry. *Journal of Metamorphic Geology*, **26,** 155–179.

Prigogine, I. & Defay, R.F., 1954. *Chemical Thermodynamics*. Longmans Green, London.

Ridley, J. & Thompson, A.B., 1986. The role of mineral kinetics in the development of metamorphic microtextures. In: *Fluid-Rock Interactions During Metamorphism* (eds Walther, J.V. & Wood, B.J.), *Advances in Physical Geochemistry*, **5,** Springer-Verlag, New York, 154–193.

Rubie, D.C., 1986. The catalysis of mineral reactions by water and restrictions on the presence of aqueous fluid during metamorphism. *Mineralogical Magazine*, **50,** 399–415.

Rubie, D.C., 1998. Disequilibrium during metamorphism: the role of nucleation kinetics. In: *What Drives Metamorphism and Metamorphic Reactions?* (eds Treloar, P.J. & O'Brien, P.J.), *Geological Society of London Special Publication*, **138,** 199–214.

Thompson, J.B., 1957. The graphical analysis of mineral assemblages in pelitic schists. *American Mineralogist*, **42,** 842–858.

Thompson, A.B., 1976. Mineral reactions in pelitic rocks: I. Prediction of P-T-XFe-Mg phase relations. II. Calculation of some P-T-XFe-Mg phase relations. *American Journal of Science*, **276,** 401–424.

Thompson, A.B., 1983. Fluid-absent metamorphism. *Journal of the Geological Society of London*, **140,** 533–547.

Thompson, C.V. & Spaepen, F., 1983. Homogeneous crystal nucleation in binary metallic melts. *Acta Metallurgica*, **31,** 2021–2027.

Tinkham, D.K. & Ghent, E.D., 2005. Estimating *P–T* conditions of garnet growth with isochemical phase diagram sections and the problem of effective bulk-composition. *Canadian Mineralogist*, **43,** 35–50.

Vernon, R.H. & Powell, C.M., 1976. Porphyroblastesis and displacement – some new textural criteria from pelitic hornfels – reply. *Mineralogical Magazine*, **40,** 787–788.

Vernon, R.H., White, R.W. & Clarke, G.L., 2008. False metamorphic events inferred from misinterpretation of microstructural evidence and P–T data. *Journal of Metamorphic Geology*, **26,** 437–449.

Walther, J.V. & Wood, B.J., 1984. Rate and mechanism in prograde metamorphism. *Contributions to Mineralogy and Petrology*, **88,** 246–259.

Waters, D.J., 1990. Nucleation and overstepping in prograde metamorphic reactions. In: *Abstracts Volume: Textures in Metamorphic Rocks Conference*, University of Manchester, England.

Waters, D.J., 2010. Equilibrium calculation and real metamorphic process – scenes from a troubled relationship. In: Abstracts Volume: Interplay Between Thermodynamics, Kinetics and Deformation in Metamorphism Symposium; GeoCanada 2010 Conference, Calgary, Alberta.

Waters, D.J. & Lovegrove, D.P., 2002. Assessing the extent of disequilibrium and overstepping of prograde metamorphic reactions in metapelites from the Bushveld Complex aureole, South Africa. *Journal of Metamorphic Geology*, **20,** 135–149.

Wilbur, D.E. & Ague, J.J., 2006. Chemical disequilibrium during garnet growth: Monte Carlo simulations of natural crystal morphologies. *Geology*, **34,** 689–692.

Zeh, A. & Holness, M.B., 2003. The effect of reaction overstep on garnet microtextures in metapelitic rocks of the Ilesha Schist Belt, SW Nigeria. *Journal of Petrology*, **44,** 967–994.

Received 26 October 2010; revision accepted 3 June 2011.